University of Alberta

Fluorescent Hairpin Probes for the Detection of Chemically-Induced DNA Damage

by

Zahra Jama Shire

A thesis submitted to the Faculty of Graduate Studies and Research
in partial fulfillment of the requirements for the degree of

Master of Science

Department of Chemistry

Spring 2012
Edmonton, Alberta

Dedication

*All thanks and praises are due to **Allah** the lord of all that exist for granting me patience and strength. For my father Jama Hussein Shire and my mother Halimo Abdullah Arshe for all their support and patience during my Masters*

Abstract

In this thesis, we develop a sensitive, robust, accurate method to detect chemically-induced DNA damage by three therapeutic agents, cisplatin, psoralen and busulfan. The method uses fluorescence spectroscopy and fluorescent hairpin or molecular beacon probes in a hybridization assay for chemically-induced ssDNA damage probed in solution and on a microarray platform.

Damage is confirmed by matrix-assisted laser desorption / ionization time-of-flight mass spectrometry (MALDI-TOF MS) and UV absorbance spectroscopy. The decrease in fluorescence upon damage scales with the number of mutation sites, drug doses and irradiation time. All these results indicate that the hybridization probe**s** can quantitatively and selectively detect the number of DNA lesions/strand for chemically-induced DNA damage.

Finally, fluorescent hairpin probes have some limitations, particularly with regards to their modifications and costs. However, the development of easy, fast and reliable assays is essential for biological as well as clinical applications, but requires these limitations to be addressed.

TABLE OF CONTENTS

Chapter 5: Conclusions and Future Work

List of Tables

List of Figures

List of abbreviations

Abbreviation	Full name
A	Adenine
ACGH	Array-based comparative genomic hybridization
AmMC6	Amino modifier C6
3BHQ-1	Black hole quencher
BSA	Bovine serum albumin
C	Cytosine
cDNA	Complementary DNA
Cy5	Indodicarbocyanine
D	Damaged
DNA	Deoxyribonucleic acid
dsDNA	Double-stranded DNA
EDTA	Ethylenediaminetetraacetic acid
ELISA	Enzyme-linked immunosorbent assay
F	Fluorophore
FAM	6-carboxyfluorescein
FISH	Fluorescence *in situ* hybridization
G	Guanine
GC / MS	Gas chromatography / mass spectrometry
HMT	4′-hydroxymethyl-4,5′,8-trimethyl psoralen
HP_n	Hairpin (n = 1, 2, 3)

HPLC	High performance liquid chromatography
MALDI-TOF MS	Matrix-assisted laser desorption / ionization time -of-flight mass spectrometry
MB	Molecular beacon
mRNA	Messenger RNA
^{32}P-ATP	^{32}P-adenosine triphosphate
PCR	Polymerase chain reaction
[6-4] PP	[6-4] Pyrimidine pyrimidinone photoproduct
Q	Quencher
RNA	Ribonucleic acid
S_n	Sample (n = 1 - 6)
SDS	Sodium dodecyl sulphate
SMP3	Stealth spotting pins
SSC	Saline - sodium citrate solution
ssDNA	Single - stranded DNA
T	Thymine
T_m	Melting temperature
T_n	Target (n = 1 - 6)
$Tgt_{(n)}$	Target (n = 0,1,1a, 2)
Tris	Tris-hydroxymethylaminomethane
U	Uracil
UD	Undamaged
UVA	Ultraviolet A (320-400 nm)

UVB	Ultraviolet B (280-320 nm)
UVC	Ultraviolet C (100-280nm)
UV-Vis	Ultraviolet-visible

Chapter 1 Introduction

1.1 Nucleic Acids

Nucleic acids are essential biological molecules for life, and include deoxyribonucleic acid DNA and ribonucleic acid RNA. DNA is composed of four nucleobases, the pyrimidines thymine and cytosine, and the purines guanine and adenine. RNA differs from DNA (Figures 1.1 and 1.2) by the presence of uracil instead of thymine[1].

Both DNA and RNA are polymers consisting of nucleotides which are linked by 3′-5′ phosphodiester bonds. DNA and RNA differ in the structure of the sugar in their nucleotides; sugar units in RNA are riboses rather than deoxyriboses in DNA. Ribose contains a 2′-hydroxyl group.

DNA naturally is formed of two chains that wind together in a helical structure due to base-pairing interactions. This double helical structure can take three forms, A-DNA, B-DNA and Z-DNA depending on conditions, B-DNA is formed under normal conditions in living cells, whereas A-DNA and Z-DNA are formed under dehydration and high salt conditions, respectively[1].

DNA contains the information that is essential for the synthesis of proteins and RNA[2]. Genetic material, or the so-called genome, is composed of one or more molecules of DNA[2]. The genetic information is copied by enzymes during the synthesis of RNA, a process called transcription. Then, some of the RNA is translated to proteins [2].

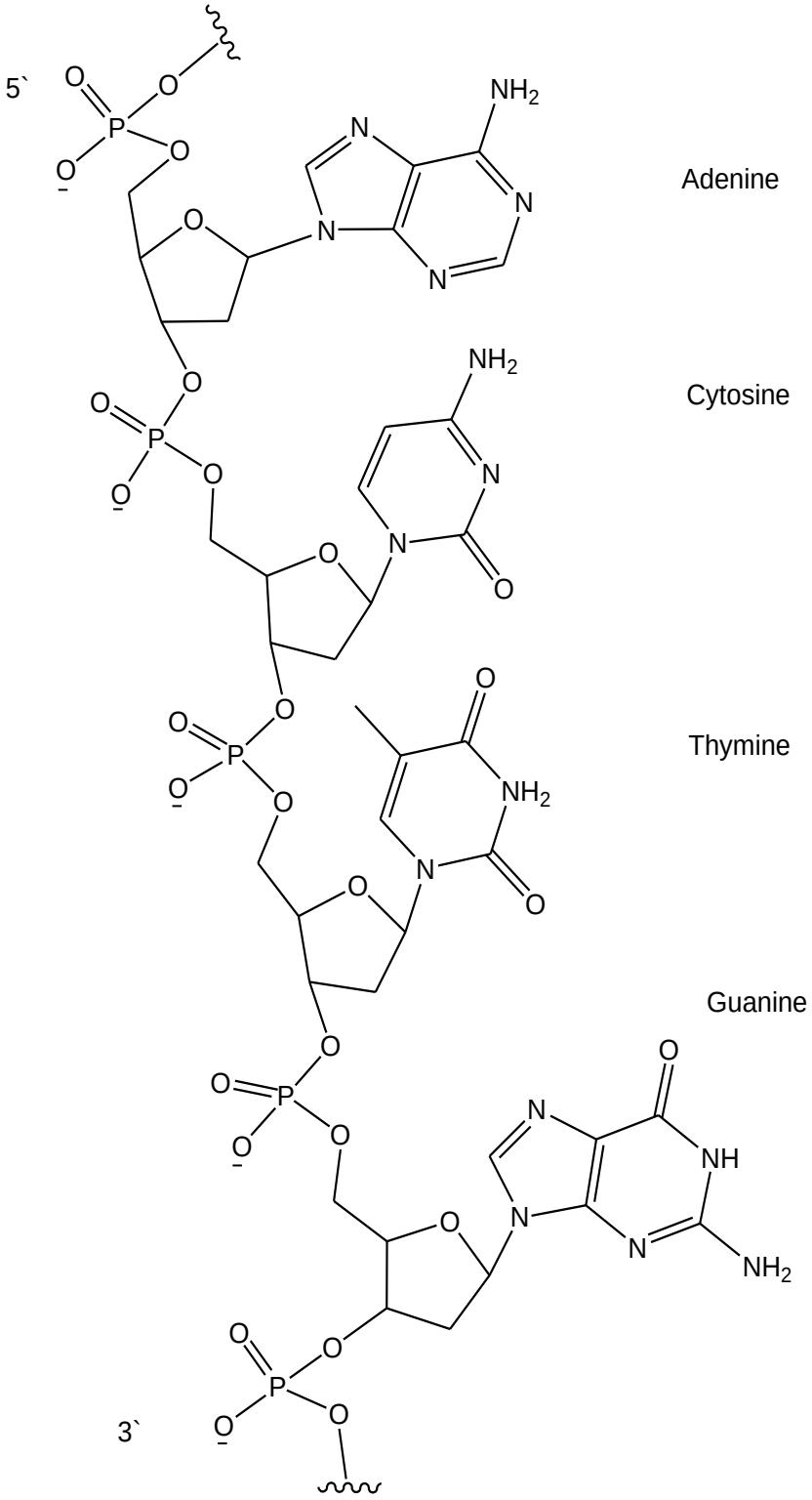

Figure 1.1 Structure of DNA

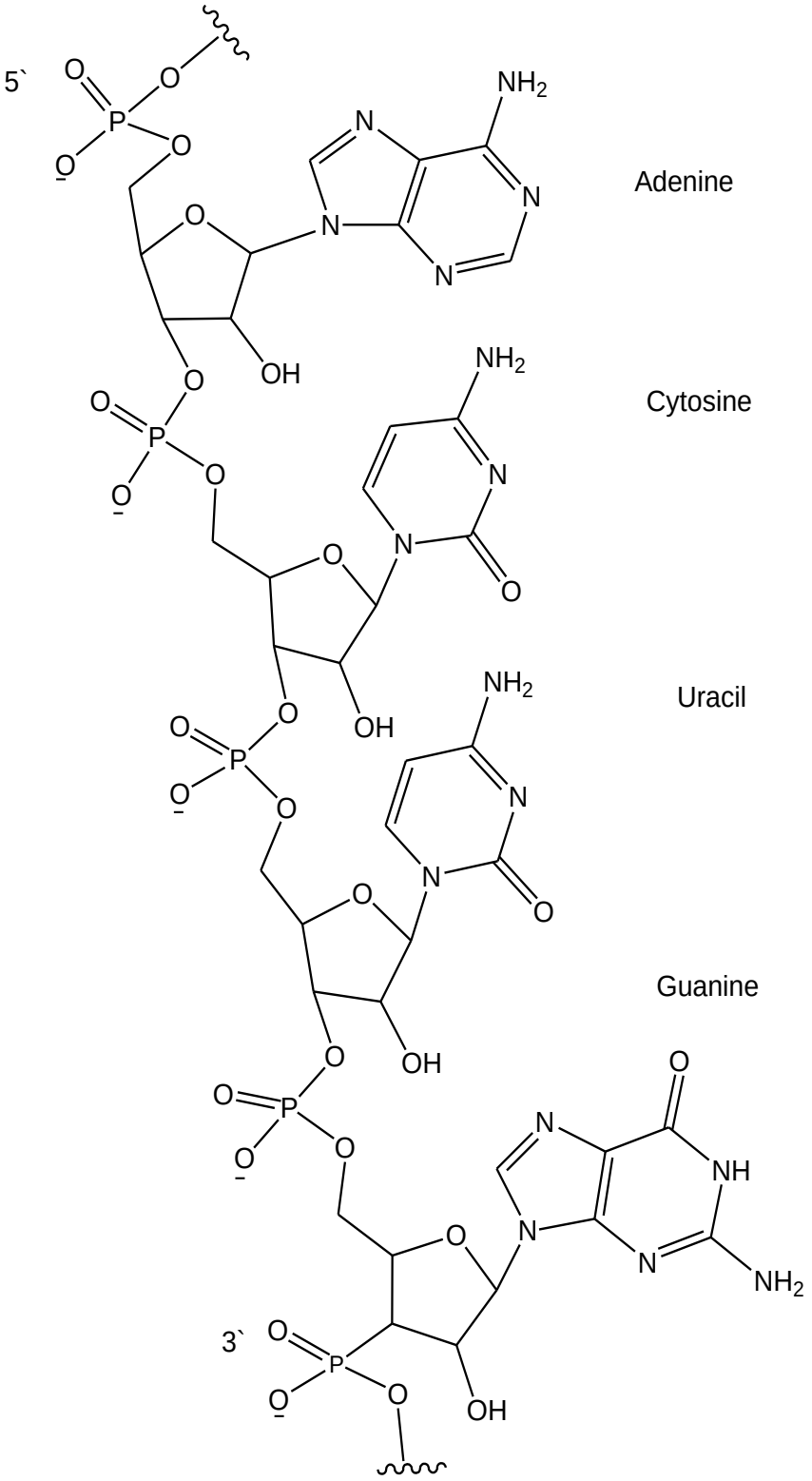

Figure 1.2 Structure of RNA

1.2 Types of DNA damage

Biological molecules like DNA and RNA are susceptible to spontaneous chemical reactions[3]. They are frequently exposed to factors from the environment or at the cellular level that may cause their damage. As a result, this damage can cause mutations that block some of the cell functions and cause the cell to be cancerous. Also, it can hinder the replication of DNA and the transcription of RNA from the genome DNA, therefore it will cause programmed cell death.

There are two sources of DNA damage. One type is endogenous factors such as reactive oxygen species which are produced from metabolic processes, and replication errors. The other is exogenous sources such as UV radiation[3, 4], ionizing radiation such as gamma-rays and x-rays, industrial chemicals, food contaminants and other chemicals from the environment such as polycyclic aromatic hydrocarbons found in smoke and tar [5-7].

DNA damage includes base loss which creates apurinic or apyrimidinic site, deamination which is the loss of amino group from the nucleic acid bases such as cytosine, guanine, and adenine[3]; these types of damage are caused by hydrolysis. Ionizing radiations can cause single and double-strands break. UV-B and UV-C lights create UV-induced photoproducts. Interstrand and intrastrand crosslinks, bulky chemical adducts are formed by the exposure of DNA to chemicals. Oxidative damage such as 8-oxoguanine[3] are caused by reactive oxygen species.

Like DNA damage due to the exposure to radiation, chemicals can induce DNA damage by endogenous and exogenous mechanisms. At the cellular level, byproducts of cellular metabolism like ubiquitous, indirect alkylation from reactive oxygen species[8-10], and enzymatic nitrosation of amines[11] can cause DNA strand breaks and oxidative damage. The exogenous chemical reagents present in food, cigarette smoke, fuel combustion products, environmental and industrial toxicants, and chemotherapeutic agents[8] produce DNA -adducts and crosslinking of DNA.

Chemotherapy is a widely used cancer treatment and is looked upon as a gentler method than radiotherapy and surgical techniques. The strategy of many cancer chemotherapies is to target the DNA of tumor cells to cause cell death or to slow the growth rate by inhibiting DNA polymerization[8, 12]. Unfortunately, the major drawback of chemotherapy is that normal cells can be affected as well.

There are several types of antitumor agents used in chemotherapy. Staurosporine is an example of type of antitumor agent that interferes with cell cycle progression by blocking kinase activity during cell replication[13-15]. Other types, such as flavopiridol and taxol can cause cell death during replication and other stages of cell cycle[16-18] or, such as cisplatin and chlorambucil by altering the structure of DNA[19, 20]. Antimetaoblites, such as gemcitabine can inhibit DNA synthesis [21].

Furthermore, DNA-binding drugs can be classified [22] as coordinative binding agents, such as groove binders that bond with either the minor or the major grooves of DNA depending on their affinity to specific sequences, intercalators, agents which intercalate between the two adjacent base pairs of the DNA helix, and, phosphodiester backbone-binders, agents which attach to the DNA by bonding with the phosphodiester group of DNA[22].

It is worth mentioning that some of the above mentioned types of agents target the same functional group in the DNA bases (Figure 1.3), the exocyclic nitrogens and oxygens, and aprotic ring nitrogens[8]. Furthermore, the N_7 and O_6 of guanine and N_3 of adenine are common sites for alkylation by a number of chemotherapeutic agents, and the most accessible site for alkylation is N_7 position [23, 24]. The mechanism of action of the alkylating reagents is divided into two categories[8]. The first group follows the S_N1 reaction which is a first order kinetic reaction that depends on forming a carbonium ion as an intermediate. The second group involves S_N2 reaction, a second order reaction which depends on both the alkylating reagent and the DNA.

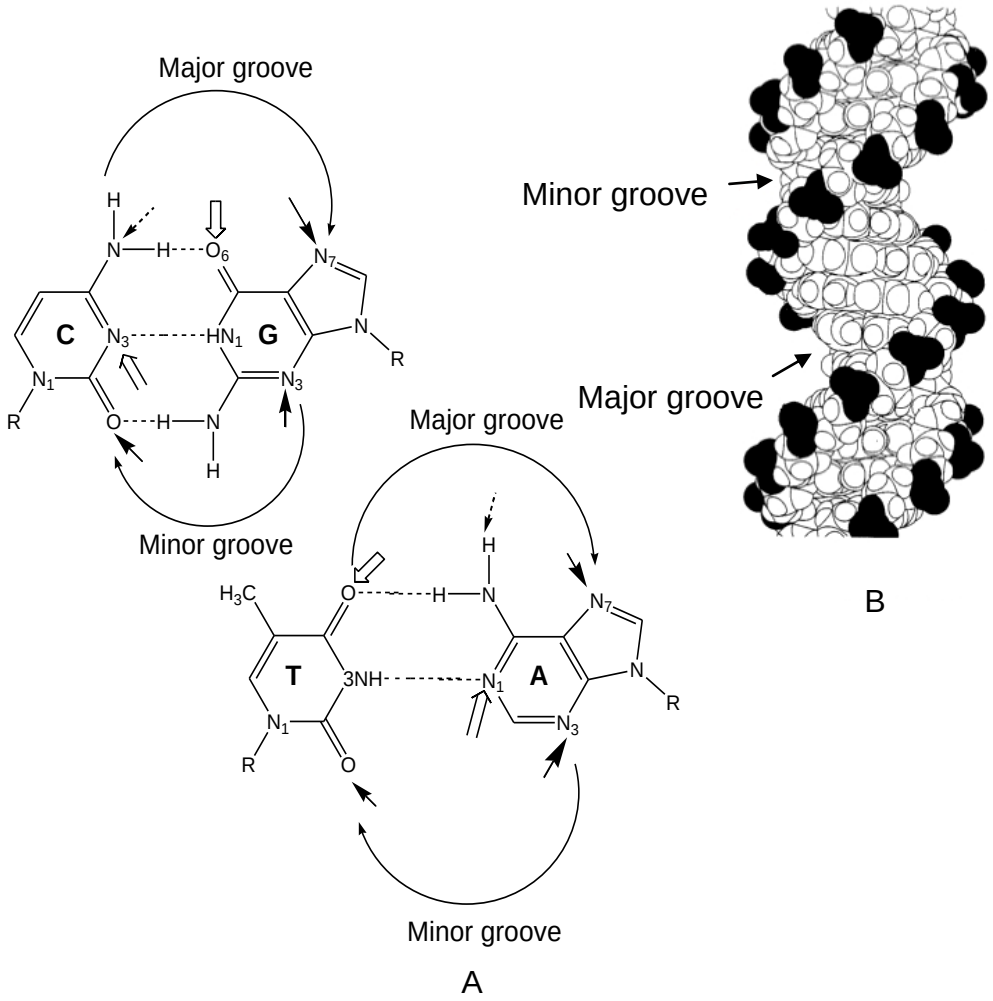

Figure 1.3 (A) Targeted sites of DNA bases by damaging agents. The different arrows indicate the exocyclic nitrogens, oxygens and ring nitrogens without hydrogens. White closed arrows indicate sites attacked by S_N1 reagents, and white open arrows indicate sites attacked by S_N2 agents in ssDNA. Dashed black arrows indicate exocyclic amino groups, and the black arrows indicate sites attacked by S_N2 agents of the ssDNA. (B) Side view of dsDNA.

Figure 1.3 (B) obtained from http://www.chem.ucla.edu/harding/IGOC/M/major_groove.html

Cisplatin (cis-diammminedichloroplatinum(II)) is a common platinum complex-antitumor drug that is used mainly for the treatment of ovarian, testicular, and head and neck cancers (Figure 1.4) [25, 26]. Hydrolysis of the chloride ligands activates cisplatin. After this activation, cisplatin will react with cellular nucleophiles, such as sulfhydryl groups in proteins and the nucleophilic groups on nucleic acids to form DNA-protein crosslinks, DNA monoadducts, and interstrand and intrastrand crosslinks. These adducts induce cell death by triggering apoptosis [27, 28]. Cisplatin specifically targets the N_7 of adjacent purines through the formation of a coordination bond [22, 27, 29].

Busulfan (Figure 1.5) is another anticancer bifunctional-alkylating agent that causes DNA damage. It is widely used in the treatment of chronic myelogenous leukemia and for myeloablation prior to bone marrow transplantation [30]. Busulfan can putatively cause DNA damage by producing a crosslink in two adjacent guanine bases, as was suggested by a chromatographic study [31, 32]. Also, busulfan has been suggested to cause mono-alkylation and intrastrand crosslink mainly at 5′-GA-3′ and secondly in 5′-GG-3′ [33].

Psoralens, such as 4′-hydroxymethyl-4,5′,8-trimethyl psoralen (HMT), are another agent that have been shown previously to interact with nucleic acids (Figure 1.6). They are heterocyclic aromatic compounds

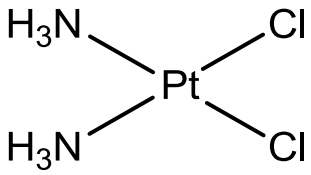

Figure 1.4 Cisplatin (cis-diamminedichloroplatinum(II)).

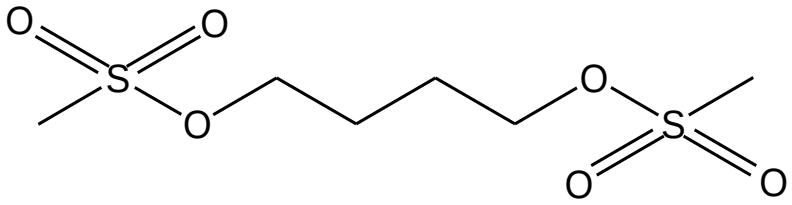

Figure 1.5 Busulfan (1,4-butanediol dimethanesulfonate).

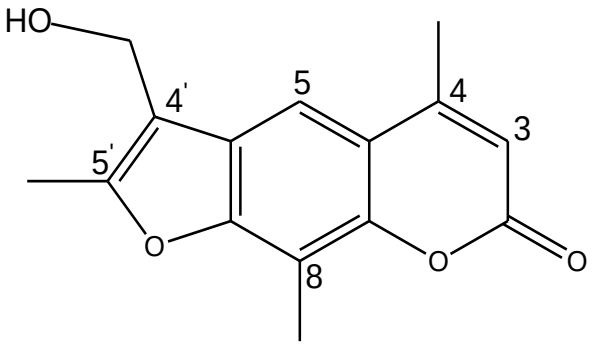

Figure 1.6 4′-hydroxymethyl-4,5′,8-trimethyl psoralen (HMT).

which absorb heavily in the UVA region (320-380 nm) [34]. This phototherapeutic agent is commonly used with the combination of UVA light to treat psoriasis and vitiligo [35, 36], but it may cause cutaneous squamous cell carcinoma and melanoma [35-37]. Psoralen intercalates in DNA and, upon exposure to UVA light, forms a covalent bond with the $C_5 = C_6$ double bond of thymine [37]. Unlike the previous mentioned drugs, psoralens prefer to react with pyrimidines, particularly thymine.

1.3 Detection of DNA damage

As mentioned above, DNA is exposed to many factors which may cause damage. Because of this, many methods have been developed for the detection of DNA damage. Electrochemical methods such as cyclic voltammetry are sensitive, selective, and cost-effective techniques that have been used previously for detecting 8-oxoguanine at carbon electrodes [38, 39]. However, DNA is an electroactive substance and this method may actually introduce more lesions [40].

Polymerase chain reaction (PCR) is used [41] in detecting [6-4] pyrimidine pyrimidinone photoproducts ([6-4]-PP), where the amplification of the strand will stop at the damage site. Despite the sensitivity of this method, there is no recognition of the particular damage and PCR provides no quantitative information [42].

^{32}P postlabeling assays have been used previously for detecting DNA-adducts in biological samples [43]. The DNA is digested enzymatically, and then radiolabeled with ^{32}P-ATP in the presence of

phage T4 polynucleotide kinase [43]. Although this method is very sensitive and doesn't require a prelableling of DNA, it's laborious and time consuming.

High performance liquid chromatography (HPLC) coupled with electrochemical, mass spectrometry and fluorescence methods as a detection tools, has been used widely in the field of detecting oxidized and photo-induced DNA damage [44, 45]. This method is sensitive and specific. However, it is again laborious, and early elution can prevent the detection of oxidative damage. This type of damage doesn't alter the polarity of the damaged bases significantly. Therefore, they will co-elute with the undamaged bases [42].

In immunochemical detection, antibodies have been generated for the detection of UV-induced DNA damage [46], and later antibodies were developed to detect oxidative damage [47]. Despite the sensitivity of this method, the cross-reactivity of the antibodies with DNA bases limits the use of this type of assays for detecting DNA damage [42].

Gas chromatography-mass spectrometry has been used in detecting radiation-induced and oxidative damage [48, 49]. This method is sensitive and requires less sample volume but it requires derivitization of the sample, which may introduce additional lesions and it's only suitable for volatile samples.

Fluorescence techniques offer sensitive methods to detect DNA damage. For example, fluorescence in situ hybridization (FISH) has

been used to detect the number of copies or the mutation location in chromosomal DNA[50]. Also, a number of dyes and stains have been used in flow cytometry assays to detect chromosomal aberrations, chemical adducts to DNA and DNA strand breakage [42, 51, 52]. Halo assays are used to detect DNA damage in cells by using fluorescent dyes that intercalate in the double helix, but this technique has a limitation in the sensitivity [53, 54]. Also, an immunoassay coupled with capillary electrophoresis and laser induced fluorescence detection was used to detect benzo[a]pyrenediolepoxide-DNA adduct [55]. Time-resolved fluorescence spectroscopy was used as well for detecting DNA damage by γ-radiation [56].

1.4 Fluorescent hairpin probes

DNA hairpins are stem-loop intramolecular base pairing structures that occur in single-stranded DNA and more commonly in RNA (Figure 1.7A). The bases in the stem part are complementary to each other, and the loop part contains unpaired bases [57]. When a fluorophore is attached to the 5′-end of the hairpin, then the fluorescent hairpin probe is used to probe ssDNA attached to a surface such as on microarray slides (Figure 1.7 B), and when a quencher is also added to the 3′-end of the hairpin it will form a molecular beacon probe (Figure 1.7 C) that can be used in solution

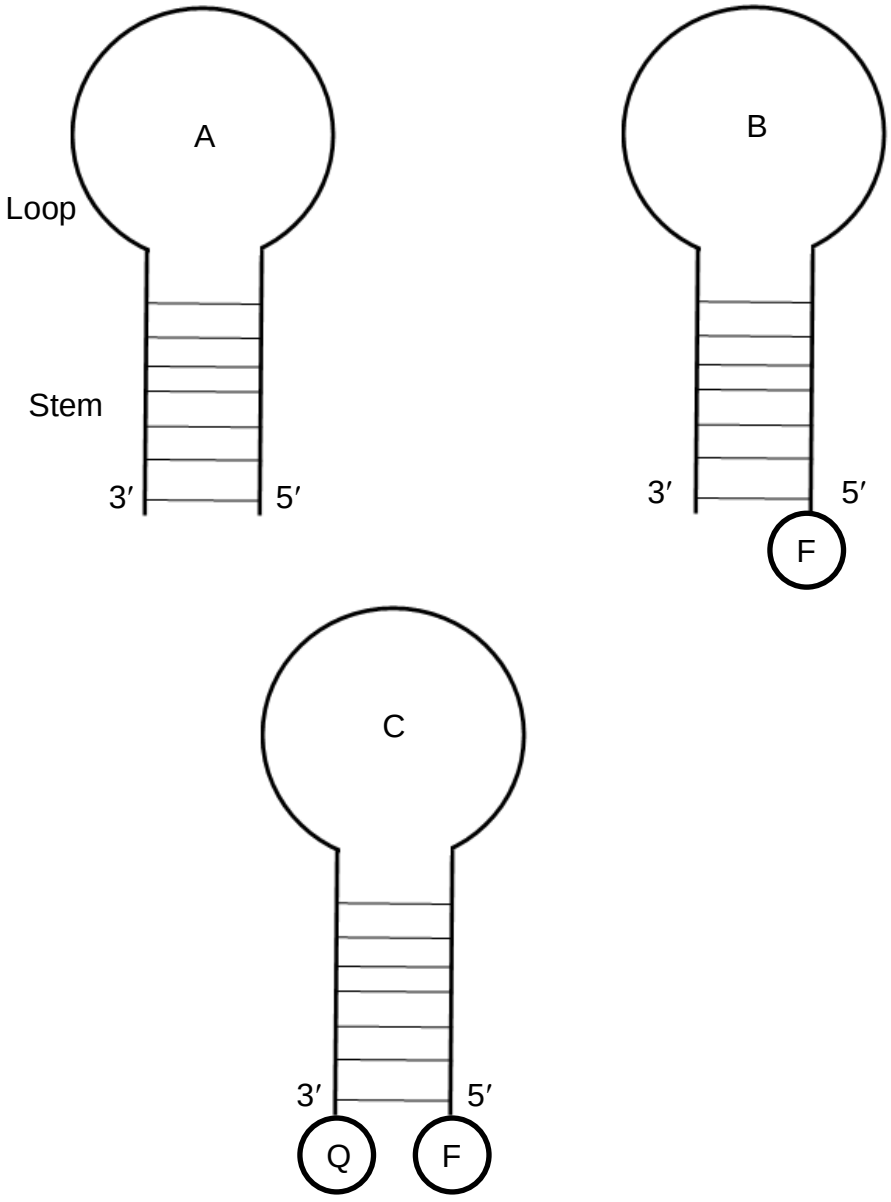

Figure 1.7 Schematic structures for (A) a structure of DNA hairpin. (B) a fluorescent hairpin probe, and (C) a molecular beacon probe. For (B) and (C) a fluorophore is attached to the 5′-end. In (C), a quencher is also attached to the 3′-end.

based assay. So what makes the fluorescent hairpin probes advantageous over fluorescent linear probes?

DNA hairpin probes have an enhanced specificity over linear DNA probes, because specificity is determined by the discrimination afforded by the balance between stem and hybrid base-pairing. This thermodynamic balance allows discrimination to a single base mismatch [58, 59]. Molecular beacon probes exhibit two stable physical states, unhybridized probe stabilized by base pairing in the stem part, and probe-target duplex stabilized by base pairing in the helix. In the presence of mismatched target, the probe-target duplex will be thermodynamically unfavourable due to the presence of the stem part of the probe which is more stable [60].

Fluorescent detection is very sensitive and, in the case of a molecular beacon probe, the sensitivity is enhanced because of the low background. In the absence of the target, the molecular beacon fluorescence is quenched. However, in the presence of a complementary target to the loop part of the molecular beacon, the probe fluorescence signal can increase by almost 2 orders of magnitude [58].

To understand better how molecular beacons work, a melting curve of one is shown in Figure 1.8 [61]. The fluorescence signal of the molecular beacon by itself is at its lowest value at low temperature because the fluorophore and the quencher are in close proximity. As

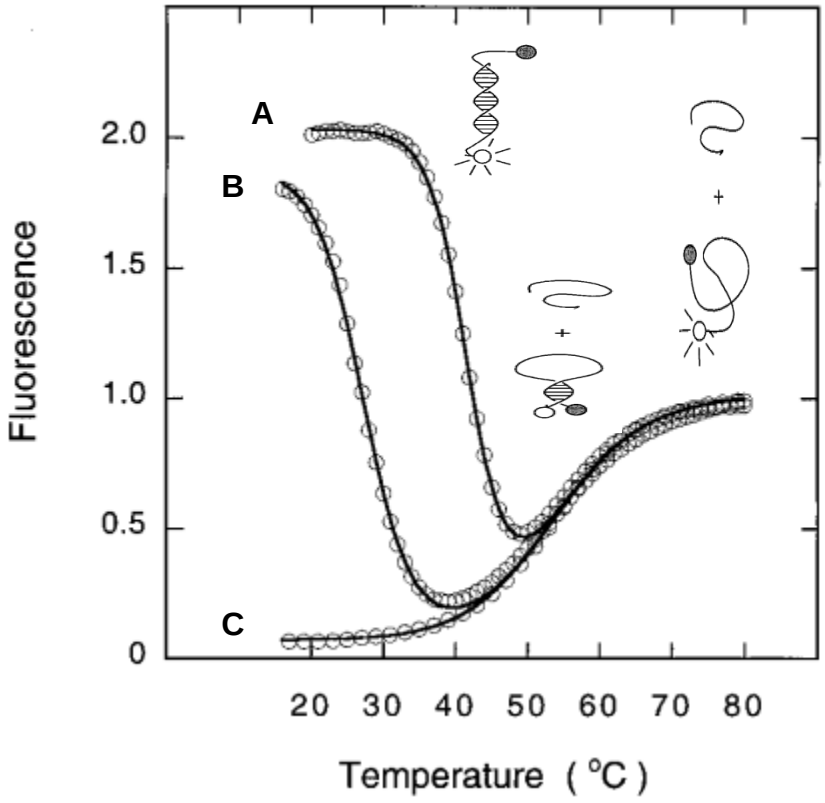

Figure 1.8 Melting curves of a molecular beacon. (A) is the curve of the molecular beacon-matched target duplex, (B) is the curve of the molecular beacon-mismatched target duplex, and (C) shows the curve of the molecular beacon probe alone. Structures of the molecular beacon are shown at various temperatures.

the temperature increases, the fluorescence signal increases as well. Above the T_m of the stem, the signal keeps increasing until it reaches a plateau. The fluorescence signal is at its highest value in the molecular beacon-matched target duplex. As the temperature increases, the duplex melts to give the closed probe and the fluorescent signal decreases. As the temperature increases further above the T_m of the stem, the molecular beacon will melt into a random coil structure and again the signal rises slightly until it reaches a plateau. The same transitions are observed for the probe-mismatched target, but with lower fluorescence signals at lower temperatures, due to lower number of hybrids formed. At these lower temperatures, the different fluorescent signals can be used to discriminate between healthy and unhealthy duplexes. Because of the given merits of the molecular beacon probes, they have been used previously in real-time monitoring of polymerase chain reaction (PCR) [62], single nucleotide polymorphism[63], and detection of mRNA in living cells [64].

1.5 DNA Microarray

Microarrays are a modification of the previously used Southern blot. The principle of DNA microarray is the hybridization of a target to a surface-attached DNA probe. DNA microarrays have helped in the fields of drug discovery, disease diagnosis, and gene expression [65-67]. The major advantages of using microarrays are cost-effectiveness, large numbers of expression products can be analyzed simultaneously,

and the ease of use [68]. The most common method used in this area is array-based comparative genomic hybridization (ACGH) [69, 70]. In this method, the DNA attached to the slide is called the probe and the extracted DNA from the cell used for the hybridization is called the target [69]. The synthesized probes are short oligonucleotides which are spotted on the surface of the microarray and then hybridized with the complementary DNA (cDNA) of the PCR product from two different cells (normal and tumor cells), that corresponds to the mRNA. The cDNA from the two different cells are labeled with different fluorophores during PCR amplification. Once the probe is hybridized with the target, the signal of detection depends on the ratiometric measurements between the two different fluorescence signals of the species on the microarray slide [71].

1.6 Summary of the Research

At present, there are several methods that are used for the detection of oxidative and UV-induced DNA damage. Although these methods have many advantages, they are time consuming, laborious, and costly. Furthermore, little work has been done to develop methods aimed at detecting chemically-induced DNA damage, particularly by therapeutic drugs. The aim of this thesis is to develop an easy, rapid and very sensitive assay by the use of highly sensitive and specific DNA recognition probes for the detection of chemically-induced ssDNA damage.

In Chapter 2, we will discuss the use of molecular beacon probes for detecting cisplatin-induced DNA damage. Psoralen-induced DNA damage is detected by using molecular beacon probes and is discussed in Chapter 3. We have found that these molecular beacons are sensitive and specific for detecting ssDNA in an easy and rapid assay without the need of isolating the undamaged as well as the extra reagents from the media.

In Chapter 4, the principle of the microarray is reversed in comparison to the original ACGH method, in which a synthetic DNA called the target, is covalently attached to the slide surface, exposed to a damaging agent, and then hybridized with the fluorescent hairpin probe. In this experiment, damage to DNA by busulfan is probed. In order to minimize the printing errors, a short labeled DNA strand called internal standard is spotted on the slide with the target DNA. The main objective of this project is to develop a fast, cost-effective and very sensitive technique for the detection of chemically-induced DNA damage. Unfortunately, the evidence of DNA damage by busulfan is conflicting.

1.7 REFERENCES

1. Davies, J.; Littlewood, B. S. *Elementary Biochemistry an Introduction to the Chemistry of Living Cell*, Prentice-Hall, Inc: New Jersey, 1979.

2. Moran, L. A.; Scrimgeour, K. G.; Horton, H. R.; Ochs, R. S.; Rawn, J. D. *Biochemistry*, 2nd ed.; Prentice-Hall, Inc: New Jersey, 1994.

3. Hoeijmakers, J. H. J. *N. Engl. J. Med*. **2009**, 361, 1475-1485.

4. Britt, A. B. *Plant Physiol.* **1995**, 108, 891-896.

5. Wei, H.; Cal, Q.; Rahn, O. R. *Carcinogenesis.* **1996**, 17, 73-77.

6. Hainaut, P.; Pfeifer, G. P. *Carcinogenesis.* **2001**, 22, 367-374.

7. Steinert, S. A.; Montee, R. S.; Sastre, M. P. *Mar. Environ. Res.* **1998**, 46, 355-358.

8. Siede, W.; Kow, Y. W.; Doetsch, P. W. *DNA Damage Recognition*. CRC press: New York, 2006.

9. Marnett, L. J.; Plastaras, J. P. *Trends Genet*. **2001**, 17, 214-221.

10. Bartsch, H.; Nair, J.; Velic, I. *Eur. J. Cancer Prev*. **1997**, 6, 529-534.

11. Taverna, P.; Sedgwick, B. *J. Bacteriol*. **1996**, 178, 5105-5111.

12. Kelley, M. R. *DNA Repair in Cancer Therapy*. Academic press: Amsterdam, 2012.

13. Harmalkar, M. N.; Shirsat, N. V. *Neurochem. Res.* **2006**, 31, 685-692

14. Koh, J.; Kubota, T.; Migita, T.; Abe, S.; Hashimoto, M.; Hosoda. Y.; Kitajima, M. *Breast Cancer*. **2002**, 9, 50-54.

15. Bonvini, P.; Zorzi, E.; Mussolin, L.; Monaco, G.; Pigazzi, M.; Basso, G.; Rosolen, A. *Haematologica*. **2009**, 94, 944-955.

16. Bridgewater, L. C.; Manning, F. C.; Patierno, S. R. *Mol. Carcinogenesis.* **1998**, 23, 201-206.

17. Randerath, K.; Randerath, E.; Zhou, G. D.; Li, D. *Mutat. Res.* **1999**, 424,183-194.

18. Cruet-Hennequart, S.; Gallagher, K.; Soko`l, A. M.; Villalan, S.; Prendergast, A. M.; Carty, M. P. *Subcell. Biochem.* **2010**, 50,189-209.

19. Wang, Y. D.; Dziegielewski, J.; Wurtz, N. R.; Dziegielewska, B.; Dervan, P. B.; Beerman, T. A. *Nucleic Acids Res.* **2003**, 31,1208-1215.

20. Donahue, B. A.; Augot, M.; Bellon, S. F.; Treiber, D. K.; Toney, J. H.; Lippard, S. J.; Essigmann, J. M. *Biochemistry*. **1990**, 29, 5872-5880.

21. Ewald, B.; Sampath, D.; Plunkett, W. *Mol. Cancer Ther.* **2007**, 6, 1239-1248.

22. Pizarro, A. M.; Sadler, P. J. *Biochimie*. **2009**, 91, 1198-1211.

23. Newbold, R. F.; Warren, W.; Medcalf, A. S.; Amos, J. *Nature*.**1980**, 283, 596-599.

24. Lawley, P. D.; Phillips, D. H. *Mutat. Res.* **1996**, 355, 13-40.

25. Gupta, R.; Beck, J. L.; Sheil, M. M.; Ralph, S. F. *J. Inorg. Biochem*. **2005**, 99, 552-559.

26. Crul, M.; van Waardenburg, R. C. A. M.; Beijnen, J. H.; Schellens, J. H. M. *Cancer Treat. Rev*. **2002**, 28, 291-303.

27. Chu, G. *J. Biol. Chem*. **1994**, 269,787-790.

28. Lippard, S. J. *Pure Appl. Chem*. **1987**, 59, 731-742.

29. Lippert, B. *Cisplatin: Chemistry and Biochemistry of a Leading Anticancer Drug*. Verlag Helvetica Chimica Acta: Zurich, 1999.

30. Probin, V.; Wang, Y.; Zhou, D. *Free Radical Biol. Med*. **2007**, 42, 1858-1865.

31. Brookes, P.; Lawley, P. D. *Biochem. J*. **1960**, 80, 496-498.

32. Tong, W. P.; Ludlum, D. B. *Biochim. Biophys. Acta*. **1980**, 608,174-181.

33. Iwamoto, T.; Hiraku, Y.; Shinji, O.; Mizutani, H.; Kojima, M.; Kawanishi, S. *Cancer Sci*. **2004**, 95, 454-458.

34. Shim, S. C. *Organic Photochemistry and Photobiology*. CRC press, Inc: New York, 1995.

35. Zhao, J. F.; Zhang, Y. J.; Jin, X. H.; Athar, M.; Santella, R. M.; Bickers, D. R.; Wang, Z. Y. *J. Invest. Dermatol*. **1999**, 113, 1070-1075.

36. Cimino, G. D.; Shi, Y. B.; Hearst, J. E. *Biochemistry*. **1986**, 25, 3013-3020.

37. Derheimer, F. A.; Hicks, J. K.; Paulsen, M. T.; Canman, C. E.; Ljungman, M. *Mol. Pharmacol*. **2009**, 75, 599-607.

38. Langmaier, J.; Samec, Z.; Samcova, E. *Electroanalysis*. **2003**, 15, 1555-1560.

39. Brett, A. M. O.; Piedade, J. A. P.; Serrano, S. H. P. *Electroanalysis.* **2000**, 12, 969-973.

40. Cahová-Kuchaříková, K.; Fojta, M.; Mozga, T.; Paleček, E. *Anal Chem*. **2005**, 77, 2920-2927.

41. Rochette, P. J.; Bastien, N.; Todo, T.; Drouin, R. *Photochem. Photobiol.* **2006**, 82, 1370-1376.

42. Kumari, S.; Rastogi, R. P.; Singh, K. L.; Singh, S. P.; Rajeshwar, P. S. *Excli Journal*. **2008**, 7, 44-62.

43. Randerath, K.; Reddy, M. V.; Gupta, R. C. *Proc. Natl. Acad. Sci.* **1981**, 78, 6126-6129.

44. Floyd, R. A.; Watson, J. J.; Won P. K.; Altmiller, D. H.; Rickard, R. C. *Free Radical Res. Comm.* **1986**, 1163-1171.

45. Wagner, J. R.; Hu, C-C.; Ames, B. N. *Proc. Natl. Acad. Sci*. **1992**, 89, 3380-3384.

46. Levine, L.; Seeman, E. S.; Hammer- Schlag, E.; Van Vunakis, H. V. *Science.* **1966**, 153,1666-1667.

47. Cadet, J.; Anselmino, C.; Douki, T.; Voituriez, L. J. *Photochem. Photobiol. B.: Biol.* **1992**, 15, 277-298.

48. Djuric, Z.; Luongo, D. A.; Harper, D. A. *Chem. Res. Toxicol.* **1991**, 4, 687-691.

49. Ramsey, R. S.; Ho, C-H. *Anal. Biochem*. **1989**, 182, 424-431.

50. Murthy, S. K.; Demetrick, D. J. *Methods Mol. Biol.* **2006**, 319, 237-259

51. Koopman, G.; Reutelingsperger, C. P.; Kuiiten, G. A.; Keehnen, R. M.; Pals, S.T. *Blood*. **1994**, 4, 1415-1420.

52. Bickham, J. W.; Sawin, V. L.; McBee, K.; Smolen, M. J.; Derr, J. N. *Cytometry*. **1994**, 15, 222-229.

53. Sestili, P.; Martinelli, C.; Stocchi, V. *Mutat. Res*. **2006**, 607, 205-214.

54. Roti Roti, J. L.; Wright, W. D. *Cytometry*. **1987**, 8, 461-467.

55. Wang, H.; Lu, M.; Mei, N.; Lee, J.; Weinfeld, M.; Le, X. C. *Anal. Chim. Acta.* **2003**, 500, 13-20.

56. Cosa, G.; Vinette, A. L.; McLean, J. R. N.; Scaiano, J. C. *Anal. Chem.* **2002**, 74, 6163-6169.

57. Cuesta-L´opez, S.; Peyrard, M.; Graham, D. J. *Eur. Phys. J. E.* **2005**, 16, 235-246.

58. Broude, N. E. *Encyclopedia of Diagnostic Genomics and Proteomics*. Marcel Dekker, Inc.: New York, 2005.

59. Cantor, C. R.; Smith, C. L. *Genomics*. Wiley & Sons, Inc.: New York, 1999.

60. Abou-ela, F.; Koh, D.; Tinoco, I.; Jr.; Martin, F. H. *Nucleic Acids Res*. **1985**, 13, 4811-4824.

61. Bonnet, G.; Tyagi, S.; Libchaber, A.; Kramer, F. R. *Proc. Natl. Acad. Sci.* **1999**, 96, 6171-6176.

62. Schofield, P.; Pell, A. N.; Krause, D. O. *Appl. Environ. Microbiol.* **1997**, 63, 1143-1147.

63. Yuan, C-C.; Peterson, R. J.; Wang, C. D.; Goodsaid, F.; Waters, D. *J. Clin. Chem.* **2000**, 46, 24-30.

64. Sokol, D. L.; Zhang, X. L.; Lu, P. Z.; Gewitz, A. M. *Proc. Natl. Acad. Sci.***1998**, 95, 11,538-11,543.

65. Heller, M. J. *Annu. Rev. Biomed. Eng.* **2002**, 4,129-153.

66. Lander, E. S. *Nat. Genet.* **1999**, 21, 3-4.

67. Wong, L. S.; Khan, F.; Micklefield, J. *Chem. Rev.* **2009**, 109, 4025-4053.

68. Koo, J.; Ko, J.; Lim, H. B.; Song, J. M. *Microchem. J.* **2011**, 99, 523-529.

69. Kallioniemi, A.; Kallioniemi, O. P.; Sudar, D.; Rutovitz, D.; Gray, J. W.; Waldman, F.; Pinkel, D. *Science.* **1992**, 258, 818-821.

70. Coe, B. P.; Ylstra, B.; Carvalho, B.; Meijer, G. A.; MacAulay, C.; Lam, W. L. *Genomics*. **2007**, 89, 647-653.

71. Fraser, K.; Wang, Z.; Liu, X. *Microarray Image Analysis: an algorithmic approach*. CRC Press Taylor & Francis group: New York, 2010.

Chapter 2 Molecular Beacon Probes for the Detection of Cisplatin-induced DNA Damage[*]

[*] A version of this chapter has been published. Shire, Z. J.; Loppnow, G. R. *Anal. Bioanal. Chem.*, **2012**, 403, 179 -184

2.1 INTRODUCTIONS

DNA damage is a frequent cellular process, causing mutations that may lead later to cancer. There are several factors that cause damage to DNA. Internal factors at the cellular level, such as replication errors, reactive oxygen species as a result of respiration[1] and other metabolic activities cause a variety of DNA damage products. External factors, including UV radiation [2, 3], ionizing radiation such as gamma-rays and x-rays, industrial chemicals, food contaminants and other environmental chemicals such as polycyclic aromatic hydrocarbons found in smoke and tar [4, 5], also cause DNA damage.

Cancer radiotherapy and chemotherapy function by damaging DNA at a rate that overwhelms the ability of the cell to repair DNA damage, which then leads to cell death. Cancer chemotherapy is looked upon as a successful tool for treating cancer, but it can have toxic side effects. For example, most treatments do not specifically target tumor cells and instead damage all cells. Cisplatin (cis-diamminedichloroplatinum(II), Figure 1.4, Chapter 1) is one of the anti-tumor drugs used to treat testicular, ovarian [6], neck, head, bladder and small lung cancers [7, 8].

Cisplatin undergoes activation via ligand exchange before binding to DNA, displacing its chloride ions with hydroxyl groups or water [9]. Activated cisplatin then reacts with cellular DNA by intrastrand crosslinking between either two adjacent guanine bases or adjacent adenine and

guanine bases [9-12]. These adducts are the major products formed by cisplatin; all other types of adducts are minor [11]. The cisplatin-DNA adducts may interfere with DNA replication, inhibit cell division and eventually lead to cell death. It is clear from this mechanism that cisplatin may also cause damage to normal cells while inhibiting the spread of cancerous cells.

Several techniques have been used previously to detect DNA damage. These methods include high performance liquid chromatography (HPLC) separation[13], gas chromatography-mass spectrometry (GC/MS) [14], ^{32}P-postlabeling analysis[15], restriction enzyme assays[16] and immunological assays[17-19]. The major drawback of the chromatographical and ^{32}P-postlabeling techniques is the need to fragment and isolate the damaged DNA from an excess of undamaged oligonucleotides, a time-consuming process and one that potentially introduces more damage. While the restriction enzyme and immunological assays are sensitive, they are also very specific. It is this specificity that makes them unsuitable for detecting general or multiple types of DNA damage in a single assay.

Molecular beacons (MBs) are ssDNA oligonucleotide probes in which the 5′ and 3′-ends are self-complementary and labeled with fluorophore and quencher, respectively [20]. They adopt a hairpin structure which, in its closed form, has little fluorescence intensity due to the proximity of fluorophore and quencher. However, in the presence of a target sequence complementary to the loop, the MB will open and

hybridize. Because the quencher and fluorophore are now separated, a fluorescence signal will be observed [21]. Equation 1 shows the equilibrium established for molecular beacon hybridization to a complementary oligonucleotide. This balance between the thermodynamics of the closed form and the hybridized form is what gives MBs their sensitivity to single base-pair mismatches [21].

$$MB_{closed} + Tgt \rightleftharpoons MB - Tgt \qquad (1)$$

Based on the sensitivity and specificity that MBs offer, MBs have been used in a number of bioanalytical applications, such as *in vitro* RNA and DNA monitoring, biosensors and biochips, and real-time monitoring of genes and gene expression in living systems [22]. Molecular beacons have also been used as sensitive and accurate probes of UV-induced DNA damage [23]. The sensitivity of MBs to UV-induced DNA damage suggests that they may also be used to detect chemically-induced nucleic acid damage. The sensitive and precise measurement of DNA damage is essential for understanding the mutagenic effects of DNA damage.

In this Chapter, we report MB probes for detecting chemically-induced DNA damage by the anti-cancer drug cisplatin. The MB probes are shown to be very sensitive and sequence-specific in detecting cisplatin-induced DNA damage. In addition, the MB mechanism of detection is not compromised by the presence of the damage agent in the assay, providing for a simple, mix-and-read assay. These results are

discussed in the perspective of using molecular beacons to probe DNA damage by any chemically-induced mechanism.

2.2 EXPERIMENTAL

2.2.1 Materials

The single strand oligonucleotide targets and the corresponding molecular beacons (Table 2.1) were synthesized and purified by Integrated DNA Technologies, Inc. (Coralville, IA, USA). The 6-carboxyfluorescein (6-FAM) fluorophore was attached to the 5′-end of the MB and the black hole quencher (3BHQ-1) was attached to the 3′-end of the MB. The oligonucleotide targets were purified by standard desalting, while the MBs were purified by HPLC. Oligonucleotide targets and MBs were used as received.

Cisplatin was obtained from Sigma-Aldrich Canada Ltd. (Oakville, ON, Canada), magnesium chloride from EMD Chemicals Inc. (Gibbstown, NJ, USA), sodium chloride from ACP Chemicals Inc. (Montreal, QC, Canada), ultrapure Tris from ICN Biomedical Inc. (Aurora, OH, USA), and EDTA from Fisher Scientific Company (Fairlawn, NJ, USA). All chemicals were used as received without further purification. Nanopure water from a Barnsted Nanopure (Boston, MA, USA) system was used to prepare all solutions. Oligonucleotide targets samples were dissolved in nanopure water, while MB samples were dissolved in buffer (50 mM NaCl, 20 mM Tris, 1 mM EDTA, 3 mM $MgCl_2$, pH 7.5). Both samples were kept frozen at -20 ^{o}C until needed. To anneal the MBs before hybridizing with target

Table 2.1 Sequences of oligonucleotides and their molecular beacons

Name	Sequence[a]	Molecular Beacons[b]
Tgt_o	5′- TTT TTT TTT TTT TTT TT -3′	5′- 6-FAM/ CTT CCA AAA AAA AAA AAA AAA AGG AAG /3BHQ-1-3′
Tgt_1	5′-TTT TTT TGG TTT TTT TT-3′	5′- 6-FAM/CAT TCC AAA AAA AAC CAA AAA AAG GAA TG /3BHQ-1-3′
Tgt_{1a}	5′- ACA CAC GGC ACA ACA-3′	5′- 6-FAM/ CCC AAC CTG TTG TGC CGT GTG TGG TTG GG /3BHQ-1-3′
Tgt_2	5′- TAG TTT TAG TTT TTT TT-3′	5′- 6-FAM/ CAT CCA AAA AAA ACT AAA ACT AGG ATG /3BHQ-1-3′

Oligonucleotide target sequences and molecular beacons sequences used in this study. [a]The target sequences were synthesized to have different positions of crosslinking by cisplatin (underlined bases). [b]The underlined bases in the molecular beacons are the bases that form the stem. 6-FAM is the fluorophore attached at 5′-end of the probe and 3BHQ-1 is the quencher attached to the 3′-end of the probe.

oligonucleotides, the MBs were dissolved in buffer, and were heated in a water bath to 80 ^{o}C, and then left to cool down at room temperature. For safe handling, vapor mask and gloves should be worn when dealing with cisplatin.

2.2.2 Methods

MALDI-TOF mass spectrometry.

Reaction mixtures of each oligonucleotide target with cisplatin (target : drug = 1:1), dissolved in nanopure water were incubated at 37 ^{o}C for 12 h. After incubation, the reaction mixtures and the matrix 9:1 (2,4,6-trihydroxyacetophenone : diammonium citrate) were loaded onto a sample plate for analysis. Other sample mixtures of pure oligonucleotide targets were prepared identically as controls. The molecular masses of the oligonucleotide adducts and control oligonucleotides were analyzed by using MALDI-TOF mass spectrometry, performed on a MALDI-TOF-Mass spec-Elite Voyager (Lancashire, United Kingdom) spectrometer equipped with a nitrogen laser (337 nm, 3 ns pulse and 20 Hz maximum firing rate).

Fluorescence measurements.

To obtain fluorescence measurements, the MB-target oligonucleotide (1:10) hybridization mixtures were prepared as follows. Aliquots of the target oligonucleotide-cisplatin solution were mixed with an appropriate amount of the corresponding MB and the mixtures were further diluted with Tris buffer (50 mM NaCl, 20 mM Tris, 1 mM EDTA, 3 mM $MgCl_2$, pH 7.5) to give final concentrations of 3 μM target oligonucleotide and 0.3 μM

MB. The sample mixtures were then incubated in the dark at room temperature for 12 h. Fluorescence spectra of the incubated sample mixtures were measured using a Photon Technology International Inc. fluorimeter (Lawrenceville, NJ, USA) at room temperature. The emission spectra were recorded between 490-700 nm with excitation at 480 nm. A 10-mm path length suprasil quartz fluorescence cuvette of 300 µL volume capacity was used for these measurements. Thermal denaturation profile experiments were also carried out on solutions of the same composition by varying the temperature from 20-80 ^{o}C in 4 ^{o}C steps, and a heating rate of 1 ^{o}C/min with a 5 min settling time at each time interval. The single measurements of fluorescence were performed using Tecan Safire fluorescence plate reader (Vienna, VA, USA), in which the temperature was kept at 37 ^{o}C for all the samples.

2.3 RESULTS and DISCUSSIONS

2.3.1 MALDI-TOF MS analysis of DNA adducts formed by cisplatin.

To ensure that cisplatin damages DNA, MALDI-TOF MS was performed on all the oligonucleotides used in this study. Figure 2.1 shows the mass spectrum of oligonucleotide Tgt_2 in the absence and presence of equimolar concentrations of cisplatin. The signal at m/z = 5176 amu is the molecular ion of Tgt_2 alone. Smaller side-peaks in Figure 2.1A represent the molecular ion non-covalently complexed with one or more sodium (m/z = 23 amu) and/or potassium (m/z = 39 amu) ions. In Figure 2.1B, the

signals at m/z = 5404 amu and m/z = 5630 amu indicate the addition of one and two molecules of cisplatin, respectively, to the ssDNA target after 12 h of incubation. Again, the side-peaks represent non-covalent complexes with one or more sodium and/or potassium ions. Tgt_2 has two possible sites for cisplatin adduct formation (Table 2.1). The MALDI-TOF MS of Tgt_2 immediately mixed with cisplatin was also taken as a control (Figure 2.1C). The MS obtained was similar to that of Figure 2.1A with the appearance of a small peak at m/z = 5404 which indicates the addition of a small amount of cisplatin to Tgt_2. The same procedure was performed on the rest of the sequences (see Appendix). For some of the targets, intense peaks of target-cisplatin adducts are observed immediately after mixing. These results indicate that either the MALDI-TOF is sensitive to non-covalent complexes of cisplatin with the DNA or that the kinetics of cisplatin addition are very fast compared to the 15 min time it takes to do a MALDI-TOF experiment. Nevertheless, the results provided here and in other studies [6-10] provide good evidence that DNA is damaged by cisplatin. The results here show that a single adduct of cisplatin and DNA at one of the AG sites, is the major species formed after 12 h incubation.

2.3.2 Melting curves of molecular beacons.

All MBs used in this study were carefully designed for optimum performance in detecting chemically-induced DNA damage. There are several factors that affect the performance of these nucleic acid

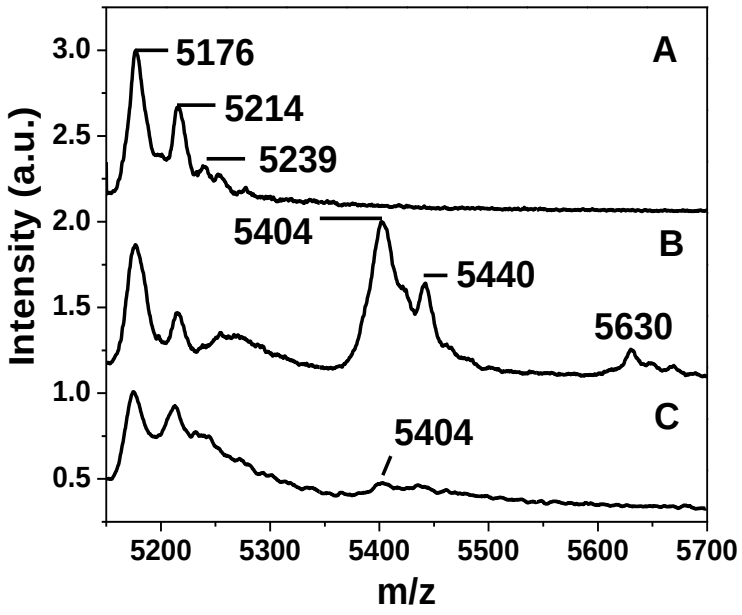

Figure 2.1 MALDI-TOF MS of Tgt_2 oligonucleotides in the absence (A) and presence (B) and (C) of cisplatin. The signal at m/z = 5176 amu indicates the molecular ion of Tgt_2. Spectrum (B) was taken after the sample mixture of Tgt_2 was incubated with cisplatin for 12 h, while spectrum (C) was taken immediately after mixing Tgt_2 and cisplatin. The signals at m/z = 5404 amu and m/z = 5630 amu indicate the addition of one and two molecules of cisplatin, respectively, to the target. Smaller peaks represent $(Na^+)_n$ and $(K^+)_n$ clusters of the target and adduct(s). The intensities have been scaled to the highest value in each spectrum and offset along the y-axis.

probes, such as the melting temperatures of the stem and the loop, the G-C content of the MB sequence and the salt concentration in the buffer solutions. All the above mentioned factors have been discussed in previous studies [20, 23, 24]. We have measured the melting curves of all the MBs used in this study to ensure that the design of our probes and conditions under which damage is measured are correct. Figure 2.2 shows the melting curves for MB_2, the MB_2 : healthy Tgt_2 hybrid and the MB_2 : damaged Tgt_2 hybrid incubated with different concentrations of cisplatin. Cooling cycles were measured as well (data not shown).

From Figure 2.2, the MB_2 alone gives an increase in fluorescence after the temperature increases more than the corresponding melting temperature of the stem. As the fluorophore and quencher of MB_2 separate, the fluorescence increases, as expected. The opposite pattern can be seen in the melting curve of the hybrid between MB_2 and healthy Tgt_2. For the hybrid, the highest fluorescence signal is observed at low temperature, which indicates that hybridization has occurred. The signal decreases as the temperature is increased, because the MB is melting off the Tgt_2 strand and reforming the closed MB, quenching the fluorescence. As the temperature continues to rise, the MB_2 stem now melts, giving rise to an intermediate fluorescent signal. As for the MB_2 : damaged Tgt_2 with different concentrations of cisplatin, the fluorescence signal is lower than

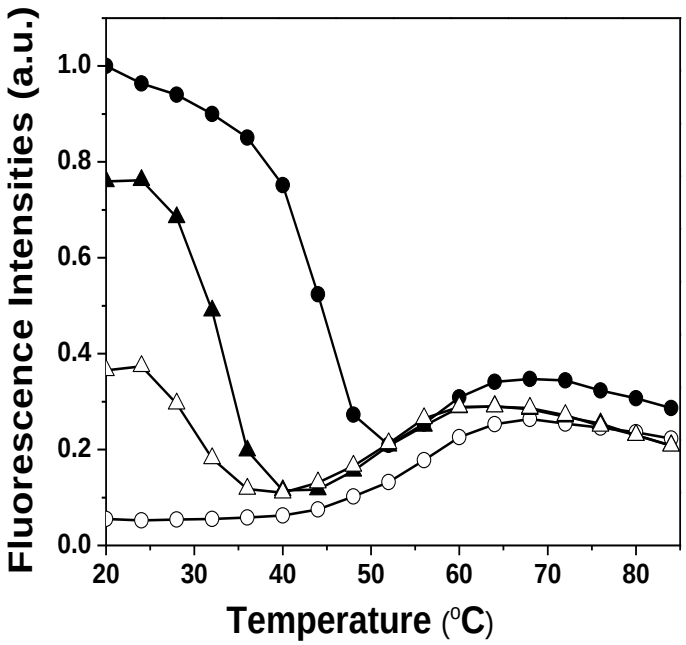

Figure 2.2 Melting curves (heating direction) for 300 nM MB_2 and 3 μM undamaged Tgt_2 hybrid (filled circles), 300 nM MB_2 and 3 μM damaged Tgt_2 by cisplatin at equimolar (filled triangles) and 2-fold excess (open triangles) concentrations, and 300 nM MB_2 alone (open circles). The fluorescence intensities have been scaled to the highest value.

in the healthy DNA : MB hybrids at low temperatures. The lower signal arises from fewer hybrids formed, due to a lower affinity of the MB for the cisplatin lesion-containing oligonucleotides. The T_m of the MB_2 : damaged Tgt_2 is also lower than in the healthy target, reflecting the lower stability of the damaged hybrid compared to the healthy hybrid. Similar behaviors in melting curves were seen for the other targets and MB probes (see Appendix).

The melting curves of the damaged targets indicate that the decrease in fluorescence upon damage scales with the cispaltin dose, due to the number of damage sites on this target. In other words, a melting curve with much fewer hybrids at low temperatures and a very low T_m is observed with a 2-fold excess of cisplatin, than with an equimolar mixture.

2.3.3 The effect of lesion numbers on the damage response.

As we have shown from the melting curve analysis (Figure 2.2), the fluorescence of MB_2 is lower in the presence of the cisplatin-DNA adduct. The same result was obtained for the other targets (see Appendix). A comparison of the fluorescence intensities between damaged and undamaged targets has been done for all the sequences used in this study, and the results are collected in Figure 2.3 shows that Tgt_o showed the highest fluorescence in the hybrid, indicating it received minimum amount of damage when incubated with cisplatin, this result is expected as Tgt_o lacks damage sites. Tgt_1 and Tgt_{1a} were incubated with equimolar amount of cisplatin. Tgt_1 and Tgt_{1a} show a similar response of MB

because they both posses one site for damage by cisplatin. Tgt_2` exhibits the least fluorescence, indicating it has the maximum amount of damage when incubated with 2-fold excess amount of cisplatin. This result is expected, as $Tgt_2$` has two possible sites for crosslinking. When Tgt_2 is incubated with equimolar of cispaltin, the damage response is similar to the response observed in Tgt_1 and Tgt_{1a}, because the amount of cisplatin added in this case is equal to half the number of damage sites in Tgt_2. This result is further confirmed in Figure 2.1, where the spectrum indicates the addition of one molecule of cisplatin is the major product, when it's incubated with equimolar cisplatin. This difference in response between Tgt_1, Tgt_{1a} and Tgt_2 at the equimolar amount of cisplatin could be due the affinity of cisplatin towards specific site. In other words, cisplatin damages GG sites more[11, 12]. From these results, we can conclude that MB probes are able to detect chemically-induced DNA damage quantitatively.

It is essential, though, to confirm that the MB : DNA hybridization is not compromised in the presence of unreacted cisplatin. In other words, is the loss of fluorescence signal observed in Figure 2.2 due to the mismatch between the hybrids or due to a disruption in the MB hybridization equilibrium by cisplatin?

Figure 2.4 shows the difference between the fluorescence intensities of MB_2 : healthy Tgt_2 hybrids, MB_2 : damaged Tgt_2 hybrids, MB_2 alone and MB_2 alone incubated with cisplatin.

For the first sample (S_1), we incubated Tgt_2 with cisplatin for 12 h, mixed the damaged Tgt_2 with MB_2, then the fluorescence intensities were measured after 12 h. For the second sample (S_2), healthy Tgt_2 was incubated with MB_2 and fluorescence intensities were measured after 12 h. From these two experiments, we conclude that MB_2 can detect damage by cisplatin, because the fluorescence intensities of MB_2 of the damaged hybrid are lower than the healthy hybrid. To check whether cisplatin interferes with the hybridization process, we mixed MB_2, Tgt_2 and cisplatin, and then measured the fluorescence immediately (S_3). The same procedure was done for MB_2 and Tgt_2 alone (S_4). From Figure 2.4, the fluorescence intensities obtained immediately after mixing MB_2 and Tgt_2 in the presence (S_3) or absence of cisplatin (S_4) were identical to the fluorescence intensities of the healthy hybrid obtained after 12 h of incubation of Tgt_2 with MB_2 (S_2), indicating that cisplatin doesn't interfere with the hybridization process. MB_2 alone was incubated with cisplatin for 12 h (S_5). MB_2 only contains GG and AG/GA sites in the stem. No increase in the fluorescence signal compared to the signal of pure MB_2 (S_6) was observed, indicating that cisplatin prefers to crosslink single-stranded DNA rather than double-stranded DNA.

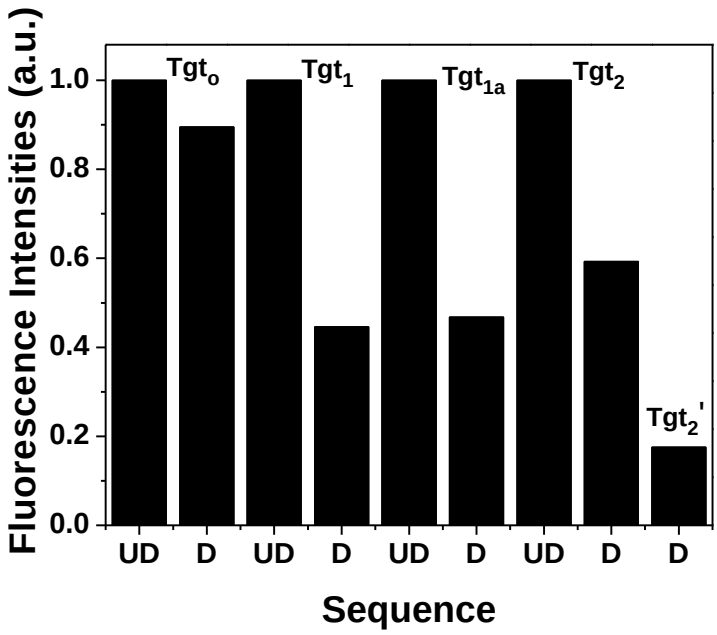

Figure 2.3 Comparison between fluorescence intensities of undamaged (UD) and damaged (D) sequences for the four targets. Tgt_2` is for Tgt_2 incubated with a 2:1 cisplatin : Tgt_2 ratio. The fluorescence intensities have been scaled to the highest value of UD level.

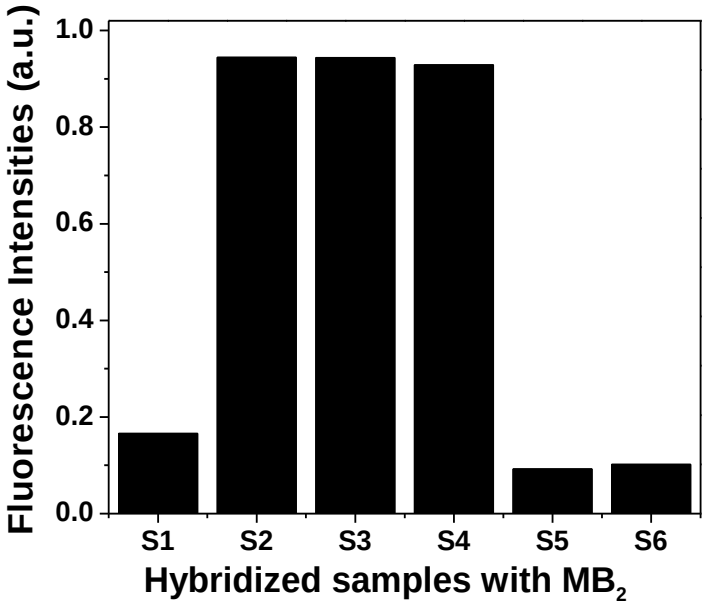

Figure 2.4 Fluorescence intensities of MB_2. 300 nM MB_2 : 3 µM damaged Tgt_2, which was incubated with 2-fold excess of cisplatin for 12 h and then was hybridized with MB_2 (S_1). 300 nM MB_2 : 3 µM Tgt_2 incubated for 12 h (S_2). 300 nM MB_2 : 3 µM Tgt_2: cisplatin (S_3), fluorescence was measured immediately after mixing. 300 nM MB_2 : 3 µM Tgt_2 (S_4), fluorescence was measured immediately after mixing. 300 nM MB_2, incubated with cisplatin for 12 h (S_5). 300 nM MB_2 (S_6). The fluorescence intensities have been scaled to the highest value

2.4 CONCLUSIONS

In conclusion, the results shown in this Chapter demonstrate the ability of molecular beacons to detect chemically-induced DNA damage by cisplatin. Our results indicate that the observed decrease in fluorescence signal is indeed due to the mismatch between the damaged target oligonucleotides and the MBs, and that the decrease correlates with both exposure to the drug and the number of cisplatin damage sites in the target strand. We have also shown that there is no disruption to the hybridization of MBs with target in the presence of the damage agent. MB probes are robust, quantitative and sensitive method for detecting chemically-induced DNA damage.

2.5 REFERENCES

1. Rowe, L. A.; Degtyareva, N.; Doetsch, P. W. *Free Radical Biol. Med*. **2008**, 45, 1167-1177.

2. Britt, A. B. *Plant Physiol*. **1995**, 108,891-896.

3. Wei, H.; Cal, Q.; Rahn, O. R. *Carcinogenesis*. **1996**, 17, 73-77.

4. Hainaut, P.; Pfeifer, G. P. *Carcinogenesis*. **2001**, 22, 367-374.

5. Steinert, S. A.; Montee, R. S.; Sastre, M. P. *Mar. Environ. Res*. **1998**, 46, 355-358.

6. Gupta, R.; Beck, J. L.; Sheil, M. M.; Ralph, S. F. *J. Inorg. Biochem*. **2005**, 99, 552-559.

7. Lippard, S. J. *Pure Appl. Chem*. **1987**, 59, 731-742.

8. Chu, G. *J. Biol. Chem*. **1994**, 269, 787-790.

9. Legendre, F.; Bas, V.; Kozelka, J.; Chottard, J. *Chem. Eur. J*. **2000**, 6, 2002-2010.

10. Bas, V.; Bombard, S.; Chottard, J.; Kozelka, J. *Chem. Eur. J*. **2003**, 9, 4739-4745.

11. Crul, M.; Waardenburg, R. C. A. M. Van; Beijnen, J. H.; Schellens, J. H. M. *Cancer Treat. Rev*. **2002**, 28, 291-303.

12. Legendre, F.; Bas, V.; Kozelka, J.; Chottard, *J. Inorg. Chem*. **1998**, 37, 3964-3967.

13. Lemaire, D. G.; Ruzsicska, B. P. *Biochemistry*. **1993**, 32, 2525-2533.

14. Fuciarelli, A. F.; Wegher, B. J.; Gajewski, E.; Dizdaroglu, M.; Blakely, W. F. *Radiat. Res*. **1989**, 119, 219-231.

15. Randerath, E.; Agrawal, H. P.; Reddy, M. V.; Randerath, K. *Cancer lett*. **1983**, 20, 109-114.

16. Thomas, D. C; Morton, A. G. Bohr, V. A.; Sancar, A. *Proc. Natl. Acad. Sci. USA*. **1988**, 85, 3723-3727.

17. Levine, L.; Seaman, E.; Hammerschlag, E.; Van, V. H. *Science*. **1966** 153, 1666-1667.

18. Santella, R. M. *Cancer Epdimol. Biomarkers Prev*. **1999**, 8, 733-739.

19. Cosma, G. N.; Miller, C. A. III; Costa, M. *Toxic in Vitro*. **1990**, 4, 17-22.

20. Tyagi, S.; Bratu, D. P.; Kramer, F. R. *Nature Biotech*. **1998**, 16, 49-53.

21. Bonnet, G.; Tyagi, S.; Libchaber, A.; Kramer, F. R. *Proc. Natl. Acad. Sci. USA.* **1999**, 96, 6171-6176.

22. Tan, L. ; Li, Y.; Drake, T. J.; Moroz, L.; Wang, K.; Li, J.; Munteanu, A.; Yang, C. J.; Martinez, K.; Tan, W. *Analyst*. **2005**, 130, 1002-1005.

23. Yarasi, S.; McConachie, C.; Loppnow, G. R. *Photochem. Photobiol*. **2005**, 8, 467-473.

24. Tyagi, S.; Kramer, F. R. *Nature Biotech*. **1996**, 14, 303-308.

Chapter 3 Molecular Beacon Probes of Oligonucleotides Photodamaged by Psoralen*

* A version of this chapter has been accepted for publication. Shire, Z. J.; Loppnow, G. R. *Photochem. Photobiol.* 2012, DOI: 1111/j.1751-1097.2012.01109.x

3.1 INTRODUCTION

Psoralens, such as 4′-hydroxymethyl-4,5′,8-trimethyl psoralen (HMT, Figure 1.6, Chapter 1) are natural products of the furocoumarin family. They have been used for the treatment of skin diseases such as psoriasis, vitiligo, and other skin pigmentation diseases[1-3]. Psoralens can intercalate between pyrimidine bases of double-stranded nucleic acids, and upon UVA (320-400 nm) irradiation, the intercalated psoralen can photoreact with adjacent pyrimidine bases [4, 5]. Monoadducts form first, with a cyclobutane ring formed between the 5,6 double bond of thymine on one strand and either the 4′,5′ (furan) or 3,4 (pyrone) double bond of the psoralen. Then, upon absorbing a second photon, it can form diadducts, linking the two strands of the double helix [4, 6]. Only the furanside monoadduct can react further with a pyrimidine on the opposite strand to create an interstrand-crosslink [7].

Photochemically-induced psoralen-DNA crosslinks may interfere with DNA replication if not repaired properly, inhibiting cell division. The photoreactivity of psoralens with nucleic acids suggests that it is a potent mutagen and may also have the potential to cause cancer [8]. Previous studies have shown that, it increases the possibility of developing cutaneous squamous cell carcinoma and melanoma [9].

DNA damage produces mutation sites that may further lead to cancer. Several methods have been developed to detect DNA damage.

Polymerase chain reaction (PCR)[10], comet assay[11], high performance liquid chromatography electrospray tandem mass spectrometry (HPLC / MS)[12], enzyme-linked immunosorbent assay (ELISA)[13], gas chromatography-mass spectrometry (GC / MS)[14], and electrochemical methods[15-17]. A major drawback for PCR and ELISA assays is the need to isolate damaged DNA from an excess of undamaged DNA[10, 13]. Electrochemical and chromatographical methods offer a sensitive and low cost detection of DNA damage. However, the procedure of these techniques may cause more lesions to DNA[14, 18]. Also, most of these techniques are time-consuming and expensive.

Fluorescent methods are sensitive and are used for both *in vivo* and *in situ* measurements of many biological molecules and processes. Fluorescent *in situ* hybridization (FISH) has been used to detect DNA damage in chromosomes[19]. Time-resolved fluorescence has also been used to detect DNA damage[20]. Recently, molecular beacons (MBs) have been used as sensitive and accurate probes of UV-induced, chemical and oxidative DNA damage [21-24, Mah, A.; Teimoory, F.; Loppnow, G. R. manuscript in preparation]. The results of these studies suggest that MBs may be used to detect psoralen-induced DNA damage.

MBs are single-stranded oligonucleotides in a hairpin shape with a fluorophore at the 5′-end and a quencher at the 3′-end. The loop part of the MB is complementary to a specific nucleic acid sequence, while the stem part consists of five to seven base pairs [25]. Fluorescence is

quenched when the MB is in the stem-and-loop structure. However, in the presence of a nucleic acid target that is complementary to the loop, the MB opens, the fluorophore and quencher separate, and the fluorescence signal increases [26]. Due to their ease of synthesis, molecular specificity, sensitivity and the ability to introduce modifications to their structure, MB probes have been used in chemistry, biology and medical sciences for molecular recognition [27-29]. A reasonable question to ask is whether MBs can detect psoralen-induced DNA damage.

In this article, we report a MB probes (Figure 3.1) specifically designed for detecting chemically-induced DNA damage by HMT. The MB probes are shown to be very selective in detecting such damage. In this work, the fluorescence of MB hybridized to UVA-activated HMT-induced dT_{17} and dA_7TTA_8 damage decreases exponentially with a single-exponential time constant of 114.2 $\pm$ 6.5 min and 677.8 min $\pm$ 180, respectively. Damage sites were further confirmed using MALDI-TOF MS measurements. Those results are discussed in the perspective of using molecular beacons to probe DNA damage by any chemically-induced mechanism for the developing of an easy, and rapid *in vitro* assays. The major concerns regarding the current study are the cost of the MB probe and the ability to use this probe for *in vivo* analysis. Future work will focus on overcoming these limitations.

3.2 EXPERIMENTAL

3.2.1 Materials

The single stranded oligonucleotide target and the corresponding molecular beacon (Figure 3.1) were synthesized by Integrated DNA Technologies, Inc. (Coralville, IA, USA). The 6-carboxyfluorescein (6-FAM) fluorophore was attached to the 5′-end of the MB and the blackhole quencher (3BHQ-1) was attached to the 3′-end of the MB. The oligonucleotide target was purified by standard desalting, while the MB was purified by HPLC. HMT (Figure 1.6, Chapter1) was obtained from Sigma Chemical Co. (St. Louis, MO, USA), magnesium chloride from EMD Chemicals Inc. (Gibbstown, NJ, USA), sodium chloride from ACP Chemicals Inc. (Montreal, QC, Canada), ultrapure Tris (tris-hydroxymethylaminomethane) from ICN Biomedical Inc. (Aurora, OH, USA) and ethylenediaminetetraaceticacid (EDTA) from Fisher Scientific Company (Fairlawn, NJ, USA). All chemicals were used as received without further purification. Nanopure water from a Barnsted Nanopure (Boston, MA, USA) system was used to prepare all solutions. Oligonucleotide target sample was dissolved in nanopure water, while the MB sample was dissolved in buffer (50 mM NaCl, 20 mM Tris, 1 mM EDTA and 3 mM $MgCl_2$, pH 7.5). Both samples were kept frozen at -20 ^{o}C until needed. Before hybridizing the MB with target oligonucleotide, the MB was dissolved in buffer and heated in a water bath to 80 ^{o}C, followed by slow cooling to anneal the MB.

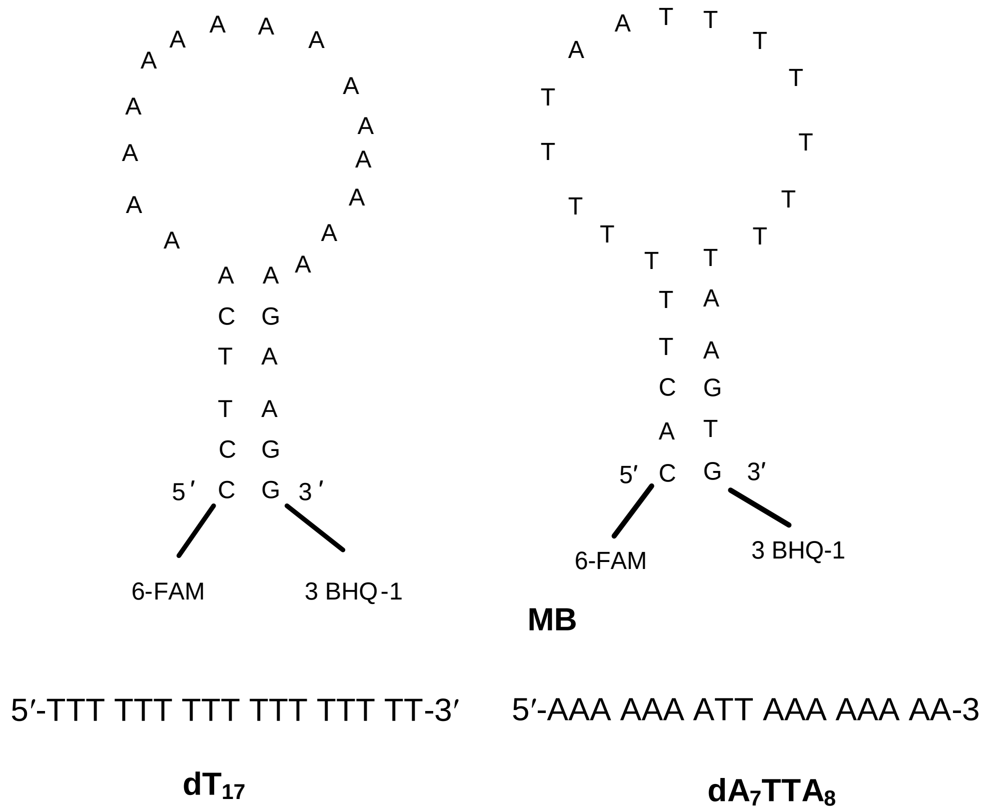

Figure 3.1 Sequences of molecular beacons and the corresponding targets.

3.2.2 Irradiation

Samples were irradiated in a Luzchem (Ottawa, ON, Canada) DEV photoreactor chamber with UV light from UVA lamps (10 lamps, energy dose 52.67 W m^{-2}), emitting over the wavelength range 316-400 nm for 0-580 min. The dT_{17} and dA_7TTA_8 solution samples consisted of 5 mL of 6 µM and 3.5 µM nitrogen-purged solutions, respectively, and were irradiated in the presence of 100 µM HMT. A quartz, 10-cm path-length cuvette sealed with a rubber septum contained the solutions used in the irradiation. The cuvettes were placed inside the chamber and were constantly stirred throughout the irradiation. The photoreactor chamber was constantly purged with nitrogen to flush out oxygen and ozone generated from the lamps. For safe handling, special goggles should be worn when using UV-photoreactor.

3.2.3 Absorption and fluorescence measurements

Absorption spectra of the irradiated samples were recorded after each irradiation period on a Hewlett-Packard 8452A diode array spectrophotometer (Sunnyvile, CA). To obtain fluorescence measurements, the MB-target oligonucleotide (1:1) hybridization mixtures were prepared as follows. A 50 µL aliquot of the sample was taken after each irradiation time, and was mixed with the appropriate amount of MB and buffer to adjust the final concentration to 100 nM targets and 100 nM MB. The hybrid mixtures were then incubated in the dark at room temperature for 16 h. Fluorescence spectra of the incubated sample

mixtures were measured using a Photon Technology International Inc. (Lawrenceville, NJ, USA) fluorimeter. The emission spectra were recorded between 490-700 nm with excitation at 480 nm. A 10-mm path-length suprasil quartz fluorescence cuvette of 300 µL volume capacity was used for these measurements. The fluorescence spectra were recorded at room temperature from a 200 µL aliquot of the hybridized mixture that contained 100 nM target oligonucleotide and 100 nM MB (50 mM NaCl, 20 mM Tris, 1 mM EDTA, 3 mM $MgCl_2$, pH 7.5). Melting curves were also measured of the MB alone and the target-MB hybrid. For these measurements, the temperature was varied from 20-80 ^{o}C in 4 ^{o}C steps at a heating rate of 1 ^{o}C/min and with a 5 min settling time between each temperature step.

3.2.4 MALDI-TOF mass spectrometry measurements

Aliqouts of 0.3 pmoles of the irradiated HMT-DNA mixture, the unirradiated HMT-DNA mixture, and a control sample of pure oligonucleotide were taken after the final irradiation time. These reaction mixtures were combined with the matrix 9:1 (2,4,6-trihydroxyacetophenone : diammonium citrate) and were loaded onto a sample plate for analysis and analyzed by using a MALDI-TOF mass spectrometer-Elite Voyager (Lancashire, United Kingdom) equipped with a nitrogen laser (337 nm, 3 ns pulse and 20 Hz maximum firing rate).

3.3 RESULTS AND DISCUSSIONS

3.3.1 UV irradiation of thymine oligonucleotides solutions

Figure 3.2 shows the absorption spectra of HMT : dT_{17} solutions irradiated by UVA light, as well as two control solutions. UVA radiation was chosen because HMT forms adduct with DNA under these irradiation conditions[1-3], but UVA radiation shouldn't directly damage DNA significantly. Control solutions of unirradiated HMT : dT_{17} and of irradiated dT_{17} alone were also prepared and their absorption spectra were measured.

No change in absorbance is observed for either the unirradiated HMT : DNA mixture (Fig. 3.2A) or for the dT_{17} alone (Figure 3.2B), indicating that light or inactivated HMT alone are insufficient to cause damage. Figure 3.2C shows the absorption of 6 µM dT_{17} incubated with 100 µM HMT and irradiated with UVA light. The absorption at approximately 330 nm is decreasing with increasing irradiation time. This region is where HMT absorbs, indicating that the HMT is producing monoadducts and / or diadducts with dT_{17}. The decrease in absorbance of HMT at 330 nm is due to the loss of $C_4' = C_5'$ or $C_3 = C_4$, whichever side interacts with thymine oligonucleotides [1, 2]. The same pattern is observed in the region around 260 nm where DNA absorbs. The loss of absorption here confirms the formation of the HMT-dT_{17} adduct. In this region the loss of absorbance is due to the loss of the $C_5 = C_6$ of the thymine nucleobases in

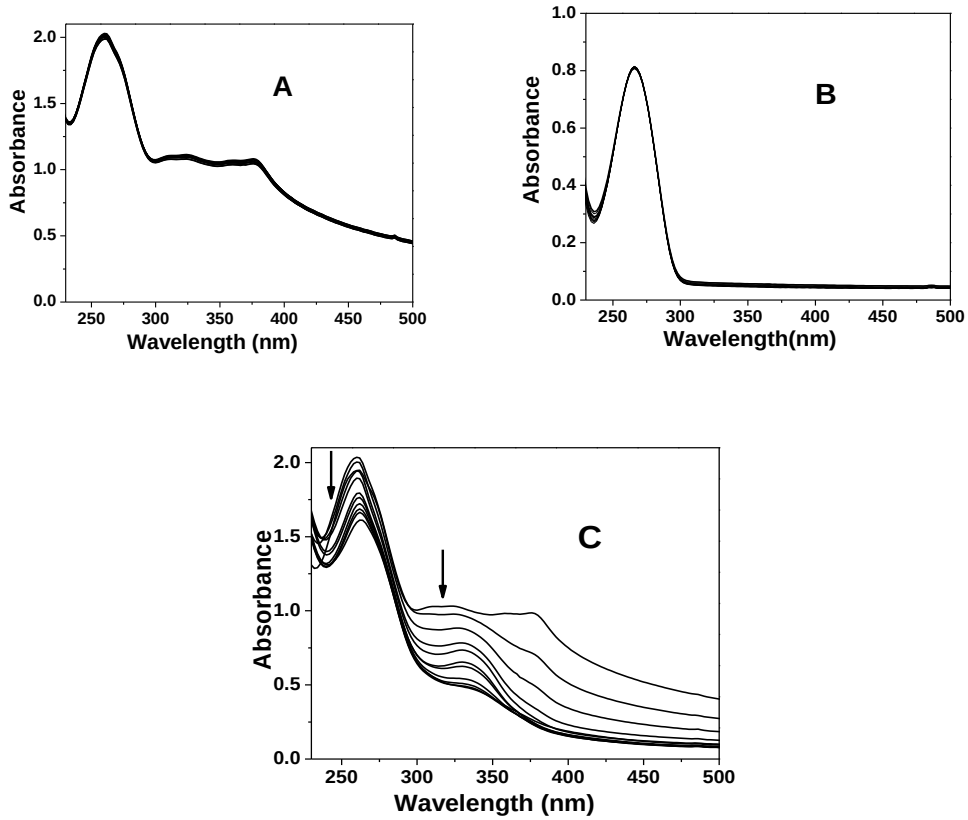

Figure 3.2 UV-Vis absorption spectra of dT_{17} solutions. (A) is the absorption spectra of a mixture of 6 µM dT_{17} and 100 µM HMT, kept in the dark. (B) is the absorption spectra of solution of 6 µM dT_{17} alone irradiated with UVA light for 0-580 min. (C) is the absorption spectra of a mixture of 6 µM dT_{17} and 100 µM HMT irradiated with UVA light for 0-580 min. In (C), the arrows indicate the direction of absorbance change with increasing irradiation time.

dT_{17} because of formation of the adducts. The absorption data are consistent with the formation of HMT : dT_{17} monoadducts and/or diadducts. The same results are observed for dA_7TTA_8 interacting with HMT (see Appendix).

3.3.2 MALDI-TOF MS analysis of DNA adducts formed by UVA-activated HMT

To ensure that HMT damages DNA, MALDI-TOF MS was performed on the irradiated HMT : dT_{17} mixture and controls. Figure 3.3 shows the mass spectrum of oligonucleotide dT_{17} in the absence (Figure 3.3A) and presence (Figure 3.3B) of 100 µM HMT. Figure 3.3C is the mass spectrum of the unirradiated HMT : dT_{17} mixture. The signal at m/z = 5108 amu in all the spectra is the molecular ion of dT_{17} alone. Note that the dT_{17} molecular ion peak is the species present in the spectrum of either the unirradiated mixture or the irradiated dT_{17} alone. In Figure 3.3B, the signals at m/z = 5363 amu, m/z = 5617 amu, and m/z = 5871 amu indicate the addition of one, two, and three molecules of HMT (m/z = 258 amu), respectively, to the ssDNA target after 580 min of irradiation time. These two controls Figure 3.3A and 3.3C, further confirm that dT_{17} is damaged in the presence of HMT only when it's irradiated with UVA. The broadness of the peaks is due to the linear negative mode used to detect DNA by MALDI-TOF MS.

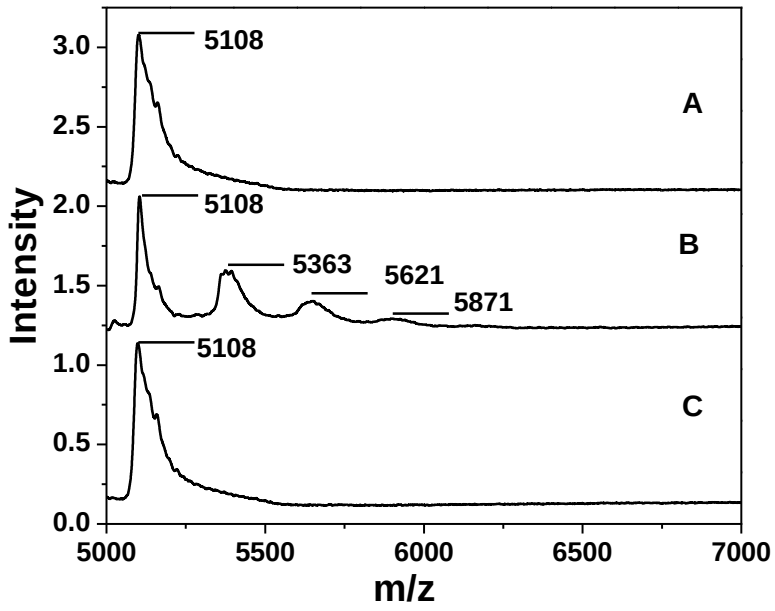

Figure 3.3 MALDI-TOF MS of irradiated dT_{17} oligonucleotide in the absence (A) and presence of HMT (C), and of irradiated HMT : dT_{17} mixture (B). Spectrum (B) was taken after the sample mixture of 6 µM dT_{17} and 100 µM HMT was irradiated for 580 min. The intensities have been scaled to highest value in each spectrum and offset along the y-axis.

3.3.3 Molecular beacons melting curves

The MB used in this study was carefully designed for optimum performance in detecting chemically-induced DNA damage. There are several factors that affect the performance of these nucleic acid probes, such as the melting temperatures of the stem and the loop, the G-C content of the MB sequence and the salt concentration in the buffer solutions, all of which have been discussed in previous studies [25-27, 29]. MBs undergo conformational changes which are temperature dependent [25]. Based on this phenomenon, we have measured the melting curves of all the MB : dT_{17} hybrids used in this study to ensure that the design of our probe is correct and that the MB detects the DNA-psoralen adduct.

Figure 3.4 shows the melting curves for the MB alone, the MB in the presence of irradiated dT_{17} in the absence of HMT as the healthy hybrid, and the MB which has been incubated with irradiated dT_{17} : HMT at different time intervals. The fluorescence signal of the hybrid of undamaged ssDNA with the MB starts at a high value, and as the temperature rises, the signal decreases, because the MB is melting off the target and reforming the closed MB. When the temperature passes the T_m of the MB stem, the fluorescence signal starts to rise again until it reaches an intermediate plateau. The MB alone shows different behavior; the fluorescence intensity is low at low temperature because the MB is in its hairpin form, and the fluorescence increases to an intermediate value as the stem melts.

For the MB which has been incubated with dT_{17} : HMT mixtures irradiated with UVA light, the fluorescence signals of the hybrid of damaged ssDNA with the MB starts at lower values than the healthy hybrid, due to fewer hybrids being formed. This result is because the MB has a lower affinity for the oligonucleotides containing HMT-thymine adducts. The fluorescence signal decreases at lower temperatures, because the hybrid is melting and the closed MB is forming again. When the temperature passes the T_m of the MB stem, the fluorescence signal starts to rise again until it reaches an intermediate plateau. The fluorescence signal at low temperature starts at a lower value, the greater the irradiation time, because more HMT-dT_{17} monoadducts and / or diadducts are formed at longer irradiation times. Note also that the T_m of the MB : damaged dT_{17} decreases as the irradiation time increases. This phenomenon indicates the increasing destabilization of the damaged dT_{17} : MB hybrid as the number of HMT adducts increases, similar results are obtained for dA_7TTA_8 (see Appendix). These results demonstrate that MBs are able to discriminate between different amounts of damage in irradiated dT_{17} : HMT mixtures.

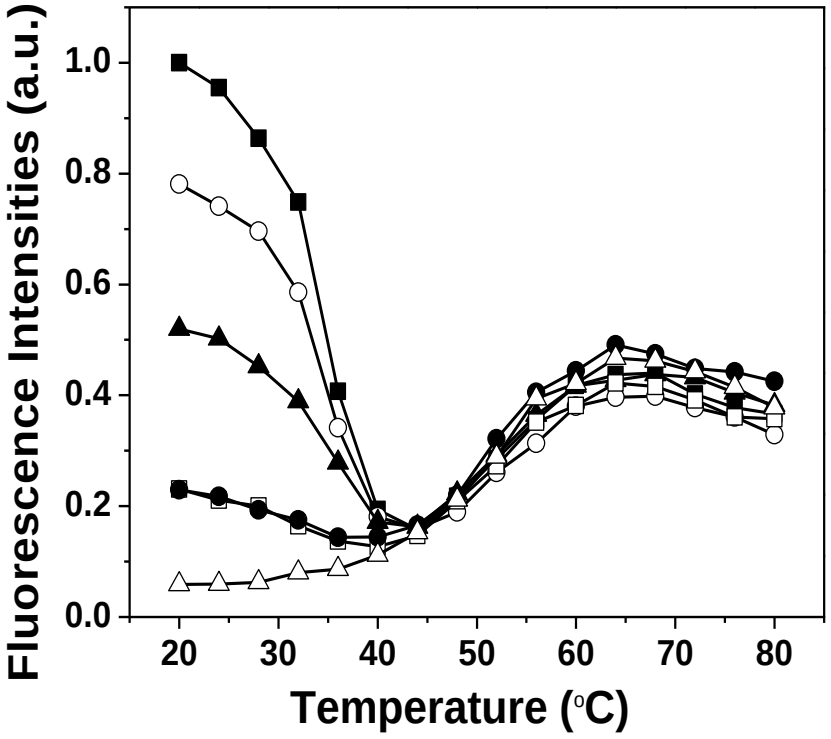

Figure 3.4 Melting curves of 100 nM MB. This figure shows the melting curves of 100 nM MB which was incubated with 100 nM dT_{17} irradiated for 0 min in the absence of HMT (filled squares), and similarly for 30 min (open circles), 90 min (filled triangles), 360 min (filled circle), and 580 min (open squares), in the presence of HMT and 100 nM MB (open triangles). The lines are simply guides to the eye. The fluorescence intensities have been scaled to the highest value.

3.3.4 MB detection of photodamaged thymine oligonucleotides by HMT

Figure 3.5 shows the fluorescence intensity of the MB as a function of irradiation time under various conditions. First, it is important to measure the background fluorescence level of the MB alone. In Figure 3.5, this signal is shown by the flat, low intensity points at the bottom of the figure. This result demonstrates the low background level of the closed MB form. The fluorescence intensities of both irradiated MB : dT_{17} in the absence of HMT and unirradiated MB : dT_{17} : HMT do not change with irradiation time, as expected. Therefore, HMT does not damage DNA in the absence of UVA light and UVA does not significantly damage ssDNA. These results are consistent with the absorption and mass spectral data present here. However, the fluorescence signal of the irradiated dT_{17} : HMT mixtures, incubated with MB, decreases exponentially due to the formation of monoadducts and / or diadducts which prevent the MB from hybridizing with dT_{17}. The fluorescence signal of the MB decreases with increasing irradiation time until it reaches approximately the fluorescence of its closed form. Under the irradiation conditions used here, we obtain a time constant of 114.2 $\pm$ 6.5 min for the MB fluorescence decrease with irradiation time for HMT-dT_{17} adducts and 677.8 $\pm$ 180 min for dA_7TTA_8 adducts (see Appendix). The results demonstrate that the MB is a selective tool to detect monoadduct and / or diadducts of HMT and dT_{17}.

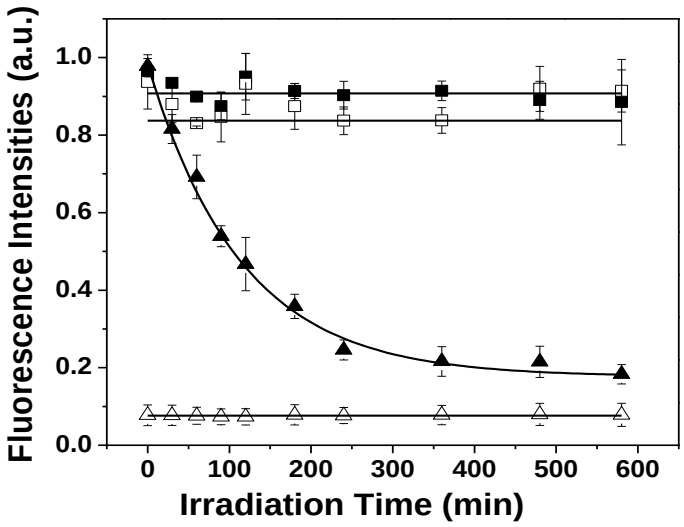

Figure 3.5 Fluorescence intensities of the MB as a function of irradiation time for 100 nM of MB alone (open triangles), 100 nM of MB incubated with 100 nM dT_{17} and 100 µM HMT kept in the dark (filled squares), 100 nM MB incubated with 100 nM dT_{17} in the presence (filled triangles) and absence (open squares) of HMT irradiated with UVA light. The solid line through the points (filled triangles) is an offset, single-exponential $y = yo + Ae^{-x / t1}$ fit. The fluorescence parameters obtained from the fit are $y_o = 0.178 \pm 0.013$, $A = 0.806 \pm 0.016$ and $t_1 = 114.2 \pm 6.5$ min. The solid lines through the points (open squares), (filled squares) and (open triangles) are linear $y = a + bx$ fit. Each data point is an average of six replicate measurements and the error bars correspond to the standard deviation of the measurements. The fluorescence curves have been normalized to the intensity of the dT_{17} : HMT : MB mixture at 0 min of irradiation. Fluorescence intensities have been scaled to the highest value.

3.4 CONCLUSIONS

The results shown in this article demonstrate the use of molecular beacons as a probe to detect UVA-activated HMT adducts of a dT_{17} oligonucleotide. Our results indicate that the observed decrease in fluorescence signal is indeed due to the mismatch between the damaged target oligonucleotides and the MBs. These results were confirmed by MALDI-TOF-MS measurements and UV/Vis absorbance spectroscopy of all the samples. MB probes are robust, quantitative and selective method for detecting chemically-induced DNA damage.

3.5 REFERENCES

1. Kim, J. H.; Sohn, S. H.; Lee, G. S.; Yang, K. S.; Hong, S. W. *Bull. Korean Chem. Soc.* **1993**, 14, 487-490.

2. Spielmann, H. P.; Sastry, S. S.; Hearst, J. E. *Proc. Natl. Acad. Sci. USA*. **1992**, 89, 4514-4518.

3. Stern, R. S. *N. Engl. J. Med.* **2007**, 357, 682-690.

4. Spielmann, H. P.; Chai, D. Y.; Hunt, N. G.; Klein, M. P.; Hearst, J. H. *Biochem*. **1995**, 34, 14801-14814.

5. Kanne, D.; Rapoport, H.; Hearst J. H. *J. Med. Chem.* **1984**, 27, 531-534.

6. Kao, J. P. Y.; Issacs, S. T.; Hearst, J. H. *Photochem. Photobiol*. **1990**, 51, 273-283.

7. Shi, Y. B.; Spielmann, H. P.; Hearst, J. H. *Biochemistry*. **1988**, 27, 5174-5178.

8. Kittler, L.; Lober, G. *J. Photochem. Photobiol. B:Biol*. **1995**, 27, 161-166.

9. Zho, J. F.; Zhang, Y. J.; Jin, X.; Athar, M.; Santella, R. M.; Bickers, D. R.; Wang, Z. Y. *J. Invest. Dermatol*. **1999**, 113, 1070-1075.

10. Rochette, P. J.; Bastein, N.; Todo, T.; Drouin, R. *Photochem. Photobiol*. **2006**, 82, 1370-1376.

11. Heepchantree, W.; Paratasilpin, T.; Kangwanpong, D. *J. Toxicol. Environ. Health.* **2006**, 69, 1072-1082.

12. Frelon, S.; Douki, T.; Ravanat , J. L.; Pouget, J. P.; Tornabene, Cadet, C. J. *Chem. Res. Toxicol*. **2000**, 13, 1002-1010.

13. Santella, R. M. *Cancer Epidemol. Biomarkers Prev*. **1999**, 8, 733-739.

14. Jenner, A.; England, T. G.; Aruoma, O. I.; Halliwell, B. *Biochem. J*. **1998**, 331, 365-368.

15. Palecek, E.; Jelen, F. *Crit. Rev. Anal. Chem*. **2002**, 3, 261-270.

16. Darain, F.; Ban, C.; Shim, Y. B. *Biosens. Bioelectron*. **2004**, 20, 857-863.

17. Rahman, M. A.; Kwon, N. H.; Won, M. S.; Choe, E. S.; Shim, Y. B. *Anal. Chem*. **2005**, 77, 4854-4860.

18. Cahová-Kuchaříková, K.; Fojta, M.; Mozga, T.; Paleček, E. *Anal Chem*. **2005**, 77, 2920-2927.

19. Sidoni, A.; Ferri, I.; Cavaliere, A.; Bellezza, G.; Scheibel, M.; Bucciarelli, E. *Anticancer Res*. **2006**, 26, 2333-2337.

20. Cosa, G.; Vinette, A. L.; McLean, J. R.; Scaiano J. C. *Anal.Chem.* **2002**, 24, 6163-6169.

21. Yarasi, S.; McConachie, C.; Loppnow, G. R. *Photochem. Photobiol*. **2005**, 81, 467-473.

22. Oladepo, S. A.; Loppnow, G. R. *Photochem. Photobiol*. **2010**, 86, 844-851.

23. El-Yazbi, A.; Loppnow, G. R. *Can. J. Chem*. **2011**, 89, 402-408.

24. Shire, Z.; Loppnow, G. R. *Anal. Bioanal. Chem*. **2012**, 403, 179 -184.

25. Tyagi, S.; Bratu, D. P.; Kramer, F. R. *Nature Biotech*. **1998**, 16, 49-53.

26. Bonnet, G.; Tyagi, S.; Libchaber, A.; Kramer, F. R. *Proc. Natl. Acad. Sci. USA*. **1999**, 96, 6171-6176.

27. Fang, X.; Li, J. J.; Perlette, J.; Wang, K.; Tan, W. *Anal. Chem*. **2000**, 72, 747A-753 A.

28. Li, J. J.; Geyer, R.; Tan, W. *Nucleic. Acids Res*. **2000**, 28, e52.

29. Tyagi, S.; Kramer, F. R. *Nat. Biotechnol*. **1996**, 14, 303-308.

Chapter 4 Detection of Busulfan-induced DNA Damage by using a Microarray Platform

4.1 INTRODUCTION

DNA microarrays are used in applications such as gene expression, disease diagnosis, drug discovery, and DNA sequencing[1-6]. They are small chips, on the size of a microscope slide, made of glass, silicon or nylon membrane, where oligonucleotide strands can be attached covalently on the modified surface of the chips in an orderly arrangement[7]. The spots can be long sequences of DNA or short oligonucleotides. This method enables a comparison of many genes to one another simultaneously, compared to the Southern blot method used before microarrays were developed. The attached DNA is usually referred to as the probes and the complementary labeled DNA strands are called the targets[7]. One of the most common methods used in this area is array-based oligonucleotide comparative genomic hybridization (ACGH), which measures two different genomic DNA, one from a tumor and the other from a normal cell [8]. The two samples are differently labeled with fluorescent dyes and then hybridized to a DNA microarray. Although microarrays have been used for gene expression studies, to the best of our knowledge, they have never been reported to be used for detecting chemically-induced DNA damage which may lead later to cancer.

Internal factors as well as external factors can cause damage to DNA. At the cellular level, replication errors, reactive oxygen species as a result of respiration [9] and other metabolic activities can cause a variety of DNA damage products. UV radiation[10, 11], ionizing radiation such as gamma-

rays and x-rays, industrial chemicals, food contaminants and other environmental chemicals such as polycyclic aromatic hydrocarbons found in smoke and tar [12, 13], may also cause DNA damage.

Anticancer drugs are used in the treatment of cancer. The mechanism of action of some of these agents relies on damaging the DNA of the tumor cell. The major drawback of these drugs is the damage they can cause in DNA of normal cells. Busulfan (Figure 1.5, Chapter 1) is a cancer drug that is used to treat chronic myelogenous leukemia and for myeloablation prior to bone marrow transplantation[14, 15]. It's a bifunctional alkylating agent which putatively forms cross-links with DNA mainly at 5′-GA-3′ and 5′-GG-3′ sequence motifs[16]. The drug reaction with cells causes damage, such as bone marrow suppression, chronic lung fibrosis, liver veno-occlusive disorder and hemorrahagic cystitis[15, 17, 18]. Because of the cytotoxicity of busulfan and other chemotherapeutic drugs towards DNA, it is essential to develop methods in order to detect DNA damage by chemical agents.

Several methods have been developed to study DNA damage. Immunological assays have been used previously for the detection of oxidative damage[19], and comet assays have been used to detect single and double strand breaks and oxidative damage [20]. An immune-coupled (PCR) polymerase chain reaction assay has been used to detect pyrimidine dimmers [21]. High performance liquid chromatography-electrospray tandem mass spectrometry (HPLC-MS) also has been used

to detect oxidative damage [22]. 8-oxoguanine has been detected by electrochemical and spectroscopic methods [23-25]. Fluorescent methods are sensitive and have been used for the detection of DNA damage previously. A common method is fluorescence *in situ* hybridization (FISH), which has been used to detect damage in chromosomal DNA [26], but which is non-specific for particular types of damage. The previous methods are advantageous tools to detect DNA damage but they have some limitations. For example, immunological assays suffer from cross reactivity of the antibodies with normal DNA bases[19]. PCR is a sensitive technique but it lacks the quantification and recognition of damage sites. Electrochemical methods are sensitive, accurate and low cost techniques but may introduce more damage to DNA[27].

DNA hairpin probes are a rapid, sensitive and selective tool that can be used for the detection of DNA damage. They consist of a stem and loop structure, the loop is complementary to the target and the stem is self complementary. A fluorophore is usually attached to the 5′-end of the strand, which allows the probe to be used for microarray hybridization[28]. Molecular beacons (MBs) are hairpin probes with a fluorophore and quencher attached to the 5′-end and 3′-end, respectively. MBs have been used as sensitive and accurate probes of UV-induced [29, 30], and oxidative DNA damage [Mah, A.; Teimoory, F.; Loppnow, G. R. manuscript in preparation]. In Chapters 2 and 3, we have shown that MBs can be used for the detection of chemically-induced DNA damage by cisplatin and psoralen, respectively.

Hairpin probes are more advantageous compared to linear DNA probes, due to their molecular specificity, sensitivity and the ability to introduce modifications to their structures [28].

In this Chapter we have combined DNA microarrays with fluorescent hairpin probes for the sensitive and robust detection of chemically-induced DNA damage by busulfan. The modification to the microarray is that the target oligonucleotides are attached to the slide surface, exposed to busulfan, and then the targets are hybridized with fluorescent hairpin probes for the detection of damage. The results obtained from the microarray analysis suggest that ssDNA are damaged, but the results obtained from MALDI-TOF MS did not support that this damage was caused by busulfan. These conflicting conclusions may indicate that perhaps the targets detach from the slides due to the treatment of the slides with busulfan, or that the differences in the fluorescence intensities are due to the difference in the amount of ssDNA printed on each spot. These suggestions are confirmed by comparing fluorescence signals of Cy5 of damaged slides with control slides and also comparing the fluorescence intensities in the FAM channel of the internal standard which reflects the amount of ssDNA printed on the slides.

4.2 EXPERIMENTAL

4.2.1 Materials

The single-stranded oligonucleotide targets and the corresponding fluorescent hairpin probes (Table 4.1 and Table 4.2) were synthesized and purified by Integrated DNA Technologies, Inc. (Coralville, IA, USA). The indodicarbocyanine (Cy5) fluorophore Figure 4.1 was attached to the 5′-end of the probe. The 5′-ends of the targets and internal standard were amino-modified and the 3′-end of the internal standard is linked to 6-carboxyfluorescein (FAM) fluorophore (Figure 4.2). The oligonucleotide targets were purified by standard desalting, while the hairpin probes were purified by HPLC. Oligonucleotide targets and probes were used as received.

Busulfan, bovine serum albumin and sodium dodecyl sulphate were obtained from Sigma-Aldrich Canada Ltd. (Oakville, ON, Canada), magnesium chloride and $Na_2HPO_4 \cdot 7H_2O$ from EMD Chemicals Inc. (Gibbstown, NJ, USA), sodium chloride from ACP Chemicals Inc. (Montreal, QC, Canada), ultrapure Tris from ICN Biomedical Inc. (Aurora, OH, USA), $NaH_2PO_4 \cdot H_2O$ and sodium citrate from Fisher Scientific (Ottawa, ON, Canada). All chemicals were used as received without further purification. Nanopure water from a Barnsted Nanopure (Boston, MA, USA) system was used to prepare all solutions. Oligonucleotide target samples were dissolved in nanopure water, while hairpin probe samples were dissolved in Tris buffer (10 mM Tris, 1 mM $MgCl_2$, pH 7.5).

Table 4.1 Sequences of oligonucleotides

Name	Sequence
T_1	5′ -AmMC6/CGC AAA TTT TTT TTT TTT TTT-3′
T_2	5′-AmMC6/GCG CCA TTG GTT GGT TGG TT-3′
T_3	5′ -AmMC6/GCG CAT TTG AGA GAG TTG AA-3′
Internal standard	5′-AmMC6/TGA GC/36-FAM/-3′

Oligonucleotide target sequences (T_1 - T_3) and internal standard sequence used in this study. The target sequences were synthesized to have different possible positions of crosslinking by busulfan (underlined bases). An amino-modified, six-carbon linker (5-AmMC6) was attached on the 5′-end to facilitate attachment to the slides.

Table 4.2 Sequences of complementary hairpin probes

Name	Sequence
HP_1	5′-/5Cy5/CGC AAA AAA AAA AAA AAA AAA TTT GCG-3′
HP_2	5′-/5Cy5/GCG CCA AAC CAA CCA ACC AAT GGC GC-3′
HP_3	5′-/5Cy5/GCG CAT TTC AAC TCT CAA ATG CGC-3′

Fluorescent hairpin probes used in this study which are complementary to targets T_1-T_3 in Table 4.1. The underlined bases in the hairpin probes are the bases that form the stem. Indodicarbocyanine, Cy5, is the fluorophore attached at the 5′-end.

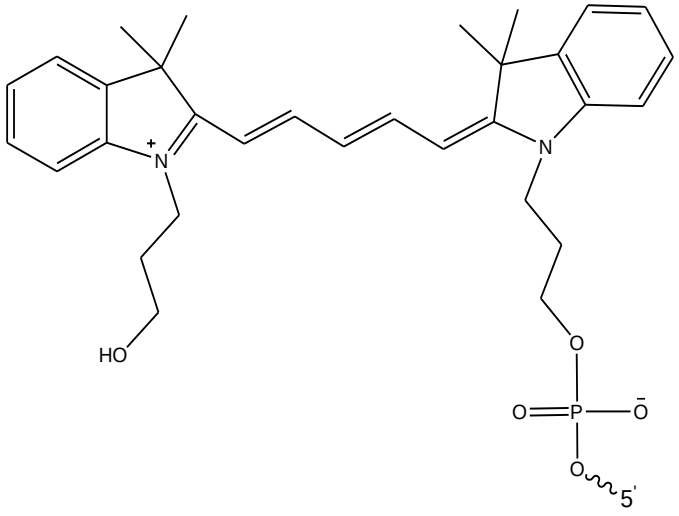

Figure 4.1 Structure of Indodicarbocyanine (Cy5) fluorophore.

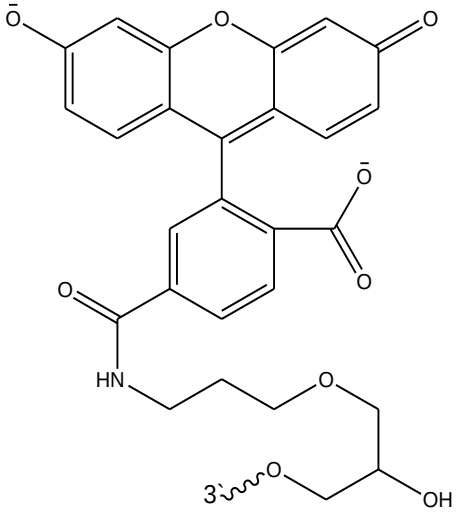

Figure 4.2 Structure of 6-carboxyfluorescein (FAM) fluorophore.

Both samples were kept frozen at -20 ^{o}C until needed. Before hybridizing hairpin probes with target oligonucleotides, the hairpin probes were dissolved in Tris buffer and were heated in a water bath to 80 ^{o}C. Then the samples were left to cool down at room temperature, annealing of hairpin probes will result in a unified structure of the probes in the buffer solution. All solutions were filtered with a 0.2 µm membrane filter.

Sample preparation. Target oligonucleotides and internal standard solutions to be printed on the slides were prepared in a 150 mM phosphate buffer (pH 8.6). The final target oligonucleotides and internal standard concentrations were 35 µM and 1 µM, respectively. The hairpin probes were dissolved in a Tris buffer (10 mM Tris, 1 mM $MgCl_2$, pH 7.5) to reach a final concentration of 5 µM. Wash 1 solution, a 0.1x sodium chloride-sodium citrate (SSC) solution, was prepared by a 200 times dilution of 20x SSC solution (3 M NaCl, 0.3 M sodium citrate, pH 7). Wash 2 solution was prepared by diluting 20x SSC and 10% SDS (sodium dodecyl sulphate) solutions in nanopure water and mixing appropriate volumes to reach a final concentration of 0.2% SDS and 2x SSC. To prepare the BSA solution (bovine serum albumin), 20x SSC, 10% SDS and 0.4 g of BSA were diluted in water to reach a final concentration of 5x SSC, 0.1% SDS and 0.2% BSA. All solutions were filtered using a 0.2 µm filter.

4.2.2 Methods

Printing and Scanning of the slides. Slide printing was done using a robotic printer in the Microarray and Proteomics Facility at the University of Alberta. The pins used for printing were made by Arrayit Corporation (Sunnyvale, CA, USA) and they are stealth spotting pins (SMP3). Each spot is 100 µm in diameter and contains 700 µL of solution. Scanning of the slides was done using a scanner made by Applied Precision Inc. (Issaquah, WA, USA). An example schematic of the microarray is shown in Figure 4.3

Treatment of the slides. After printing, the slides are left to dry and then scanned in the FAM channel to make sure all the spots of the subarrays have been printed correctly. Then the slides are treated with BSA to block the unreacted chemical groups on the slide surface in order to reduce non-specific binding. The BSA solution is preheated in a coplin jar for 1 h at 42-45 ^{o}C, and then the slides are inserted in the coplin jar and left to equilibrate for 1 h at 42-45 ^{o}C. After that, the slides are immersed three times into separate wash 1 solutions in coplin jar, at room temperature for 5 min each. After these three washes, the slides were washed in nanopure water in a coplin jar for 5 min at room temperature to remove excess SSC salt on the slides. To dry the slides from the washing steps, the slides are centrifuged for 9 min at 1400 rpm and then further dried by flowing nitrogen gas over the slides. Then the slides were scanned again in the FAM channel. The fluorescence intensities of the FAM channel taken after the BSA washing are used in the ratio between

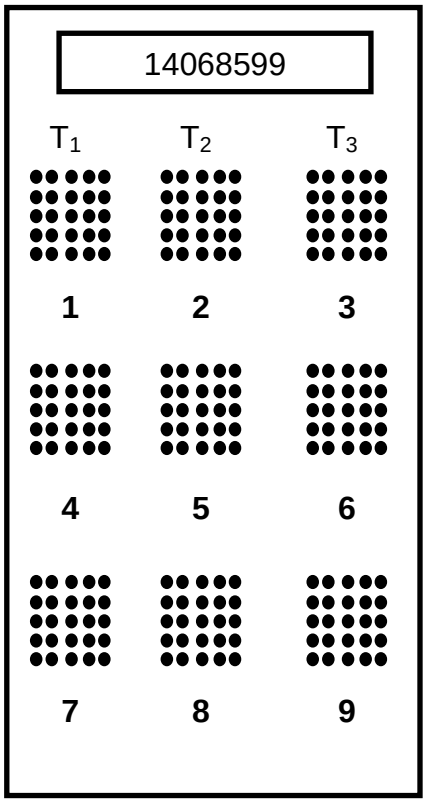

Figure 4.3 Schematic diagram of one of the slides used in this study. T_1, T_2 and T_3 are the target sequences printed in each column on the slide, and the numbers below each subarray represent the subarray numbers. The number at the top of the slide is a unique bar-code identifier for the slide. Each subarray typically consisted of 25 points.

$I_{F,\ Cy5}$ / $I_{F,\ FAM}$ to provide lower spot-to-spot errors associated with printing DNA on the microarray slides.

The exposure of the slides to busulfan. Four slides were printed for this study. Three of them were immersed in concentrations of busulfan of 100, 200 and 300 µM, while the fourth slide was kept in dry nitrogen as a control. The slides which were treated with busulfan were kept immersed in the busulfan solution for 24 h to 7 days at 37 ^{o}C to get a better damage response. After the incubation is completed, slides were washed with wash 1 followed by nanopure water. The slides were then dried using a centrifuge for 9 min at 1400 rpm and further dried by flowing nitrogen gas over the slides. For safe handling, vapor mask and gloves should be worn when dealing with busulfan.

Hybridization with fluorescent hairpin probes. Each slide was placed in a hybridization chamber. The two holes of the chamber were filled with drops of nanopure water to maintain humidity. Three drops of a buffered 5 µM probe solution (1 mM $MgCl_2$, 10 mM Tris, pH 7.5) are placed vertically along the slide, and then the slide is covered with a cover slip. The slide is then left for 16 h to hybridize. After hybridization, the slides are washed using wash 2. Before treating the slides with wash 2, the wash 2 solution is preheated at 42 ^{o}C for 1 h, and then the slides are immersed in wash 2 for 1 min each. After wash 2, the slides are treated with wash 1 three times at 42-45 ^{o}C as mentioned previously. The slides

are dried in the centrifuge at 1400 rpm for 9 min. Then the slides are scanned in both the Cy5 and the FAM channels.

Detection of busulfan-induced DNA damage by MALDI-TOF MS. Aliqouts of the busulfan-damaged DNA in solution and a control sample of pure oligonucleotides were each combined with the matrix (9:1 2,4,6-trihydroxyacetophenone : diammonium citrate) and were loaded onto a sample plate for analysis. MS analysis was done by using an Elite Voyager (Lancashire, United Kingdom) MALDI-TOF mass spectrometer equipped with a nitrogen laser (337 nm, 3 ns pulse and 20 Hz maximum firing rate).

4.3 RESULTS and DISCUSSIONS

4.3.1 The detection of the Busulfan-DNA adduct in a microarray. Microarray techniques help us to study the effect of busulfan on ssDNA more effectively than other solution-based assays, because less labour work and sample volume are required, they require less processing time, and they enable us to run multiple assays simultaneously. As a preliminary study, we have designed three targets, which have different possible positions of alkylation for attack by busulfan. Table 4.1 shows the sequences of the ssDNA used. T_1 is considered the control sequence, as there are no lesion sites for damage. T_2 was designed to have 3 -GG- positions, and T_3 has 4 -GA- positions. An amino-modified linker was attached on the 5′-end of the targets, to help attach the ssDNA to the epoxide slides. Figure 4.3 shows the slide design, with the first column

printed with T_1, the second column with T_2 and the third column with T_3. After treatment with busulfan, both the untreated control slide and the treated slide were hybridized with the probes and then scanned to get the fluorescence signals in the Cy5 channel. Figure 4.4 shows the average fluorescence intensities ($I_{F,\ Cy5}$ / $I_{F,\ FAM}$) of the control slide (filled squares) and the slide that has been treated with 100 µM busulfan (empty squares). The data obtained from both slides were combined in Figure 4.4 for comparison. The fluorescence intensities obtained from T_1 from both slides show that the difference between them is small. The fluorescence intensities of T_2 are lower compared to T_1. This result is expected because T_2 has more possible positions of alkylation and the decrease in fluorescence intensity could be due to damage by busulfan. The data obtained for T_3 also show a large difference in fluorescence intensities between the control slide and the slide treated with 100 µM busulfan. This observed decrease of fluorescence may also be due to damage by busulfan.

Figure 4.5 shows the average fluorescence intensities of the control slide (filled squares) and the slide that has been treated with 200 µM busulfan (empty squares). The fluorescence intensities obtained from T_1 from both slides again show a small difference between the control and experimental slides. The fluorescence intensities of T_2 from the experimental slide are lower than T_2 of the control slide. This result is expected because T_2 has more possible positions of alkylation and the

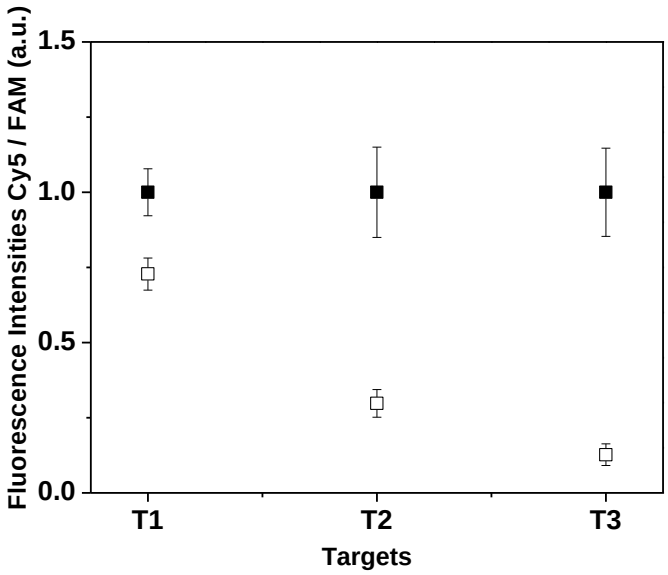

Figure 4.4 Fluorescence intensities in arbitrary units of the Cy5 / FAM intensity ratio for targets T_1-T_3 on the slide incubated with 100 µM busulfan. The filled squares correspond to data obtained from a control slide that has been kept in dry nitrogen in the dark. The empty squares correspond to data obtained from the slide which has been incubated with 100 µM busulfan. Error bars correspond to the standard deviation of the measurements. The fluorescence intensities have been scaled to the highest value.

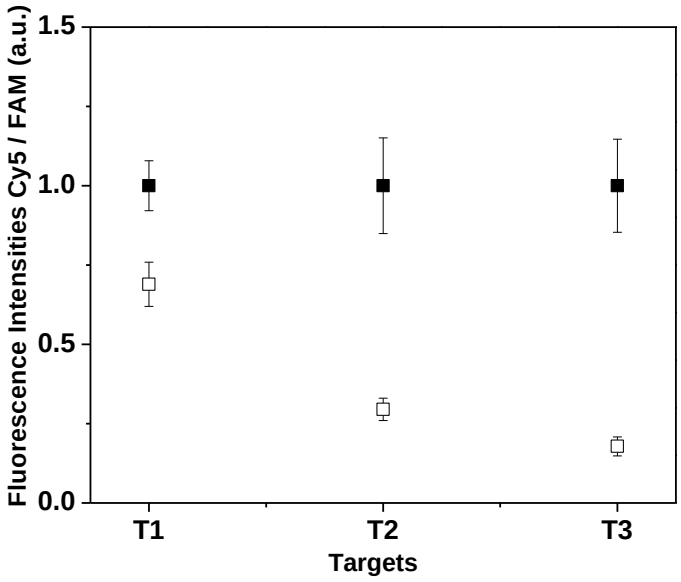

Figure 4.5 Cy5 / FAM fluorescence intensity ratios in arbitrary units of for the microarray slide incubated with 200 µM busulfan. The filled squares correspond to data obtained from a control slide that has been kept in dry nitrogen. The empty squares correspond to data obtained from the slide which has been incubated with 200 µM busulfan. Error bars correspond to the standard deviation of the measurements. The fluorescence intensities have been scaled to the highest value.

decrease in fluorescence intensity could be due to damage by busulfan. The data obtained for T_3 also show a large difference between the fluorescence intensities of the control slide and the slide treated with 200 µM busulfan. The difference in fluorescence intensities is larger for T_3 than for T_1, which may again be due to the damage caused by busulfan.

Figure 4.6 shows the fluorescence intensities of the control slide (filled squares) and the slide treated with 300 µM busulfan. The same pattern of fluorescence intensities comparison between damaged and undamaged sequences was observed for this slide as for the other 2 slides.

One common result between the different slides that have been treated with different concentrations of busulfan, is that all the slides show minimum damage of T_1. T_1 only contains T nucleobases and are less favoured for reaction by busulfan [16]. T_3 exhibits the maximum damage because GA bases are more damaged by busulfan while GG bases are damaged to a lesser extent [16]. The images of the slide treated with 100 µM busulfan are shown in Figure 4.7 after BSA treatment and in Figure 4.8 after busulfan treatment and hybridization with the probe. The remaining images can be found in the appendix.

4.3.2 Confirmation of damage by MALDI-TOF MS. To ensure that the damage observed in Figures 4.4 - 4.6 is due to busulfan addition to the ssDNA, MALDI-TOF MS was performed on all the oligonucleotides that are used in this study after incubation with 300 µM busulfan. Figures 4.9 and 4.10 are the mass spectra of T_1 in the absence and presence of

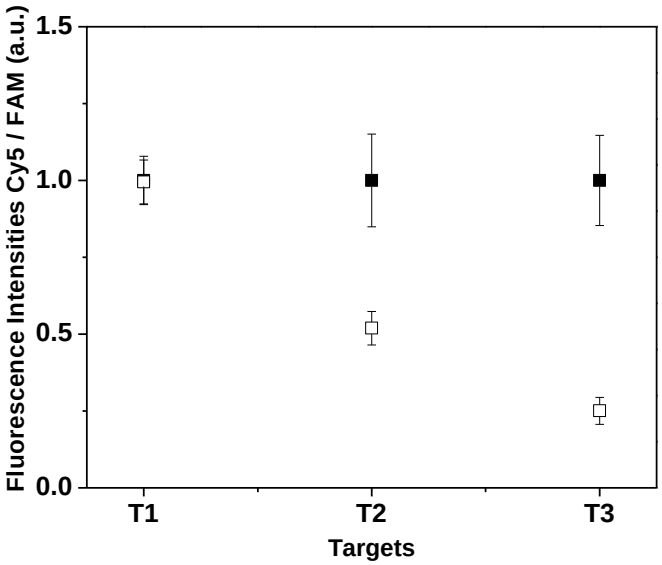

Figure 4.6 Cy5 / FAM fluorescence intensity ratios in arbitrary units for the microarray slide incubated with 300 µM busulfan. The filled squares correspond to data obtained from a control slide that has been kept in dry nitrogen. The empty squares correspond to data obtained from the slide which has been incubated with 300 µM busulfan. For T_1, the control and experimental fluorescence intensity ratios are essentially the same. Error bars correspond to the standard deviation of the measurements. The fluorescence intensities have been scaled to the highest value.

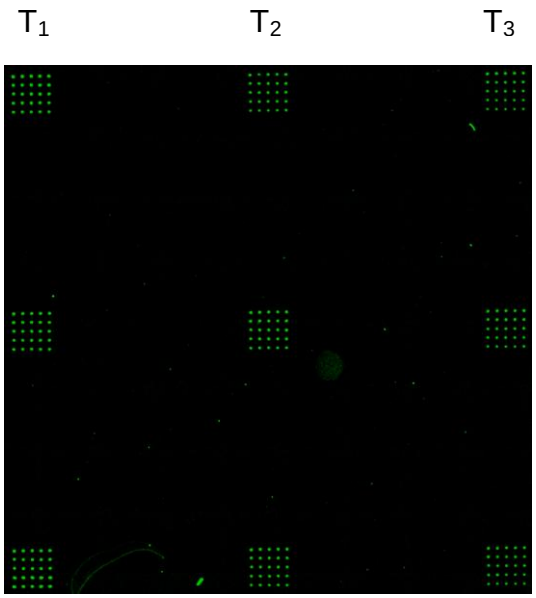

Figure 4.7 Image of the 100 µM busulfan slide after treating the slide with BSA and before treating with busulfan and probe, and scanned in the FAM channel .

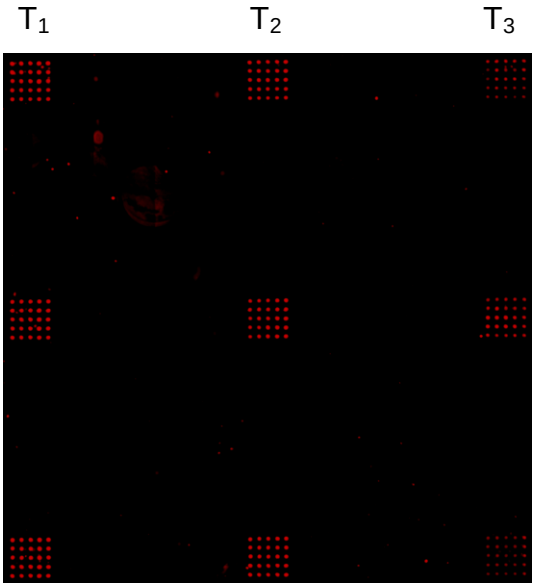

Figure 4.8 Image of the 100 µM busulfan slide treated with busulfan. The image is taken after hybridization with the probe, and scanned in Cy5 channel.

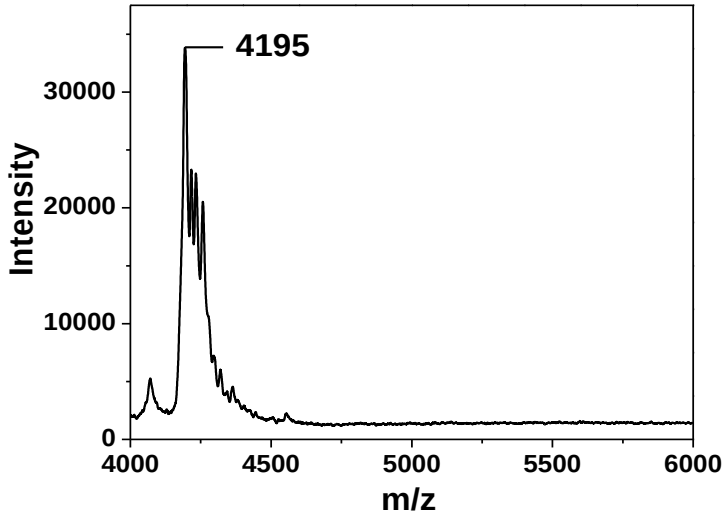

Figure 4.9 MALDI-TOF mass spectrum of control of T_1 in the absence of busulfan.

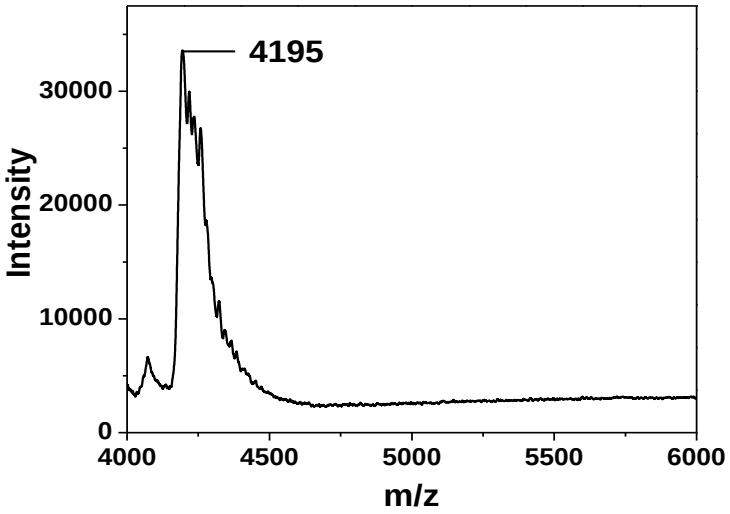

Figure 4.10 MALDI-TOF mass spectrum of T_1 after exposure to 300 μM busulfan.

busulfan respectively. The two spectra are similar to one another, which indicate that there is no addition of busulfan to T_1. This result is expected because busulfan has no or much lower affinity for thymine bases[16].

Figures 4.11 and 4.12 are the mass spectra of T_2 in the absence or presence of busulfan. Again, the two spectra are identical, which indicates no apparent addition of busulfan to T_2. The same results are observed for T_3, shown in Figures 4.13 and 4.14.

4.3.3 Factors affecting the detection signal in microarray. The results obtained from the MS analysis don't support the decrease in fluorescence signals observed in Figures 4.4 - 4.6 as arising from DNA damage. These results also indicate that busulfan doesn't interact with the ssDNA attached to the slides. Despite the fact that busulfan was mentioned previously[16] to damage ssDNA, the conclusion is that busulfan doesn't attack the DNA like the other drugs, cisplatin and psoralen explored in this thesis. Busulfan has been shown to inhibit cell growth[16]. It could be that cell growth may be affected by factors other than causing damage to the cellular DNA by busulfan because in our experiments MS measurements show no addition of busulfan to the ssDNA.

The major factor that may affect the decrease in fluorescence signal observed in Figures 4.4 - 4.6 is error in printing.

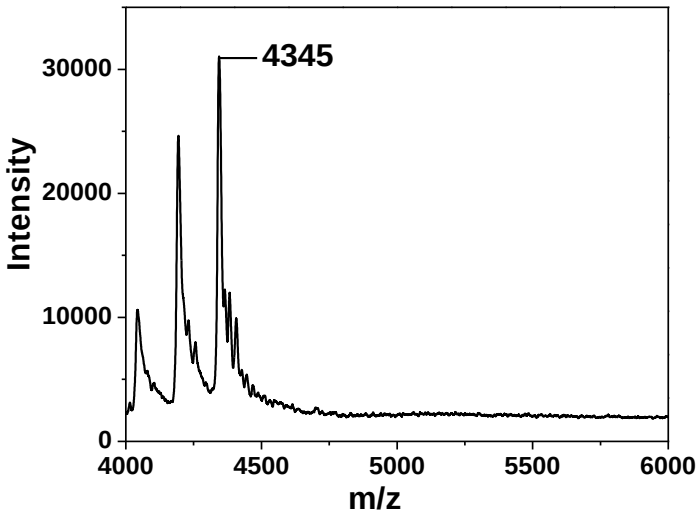

Figure 4.11 MALDI-TOF mass spectrum of control T_2 in the absence of busulfan.

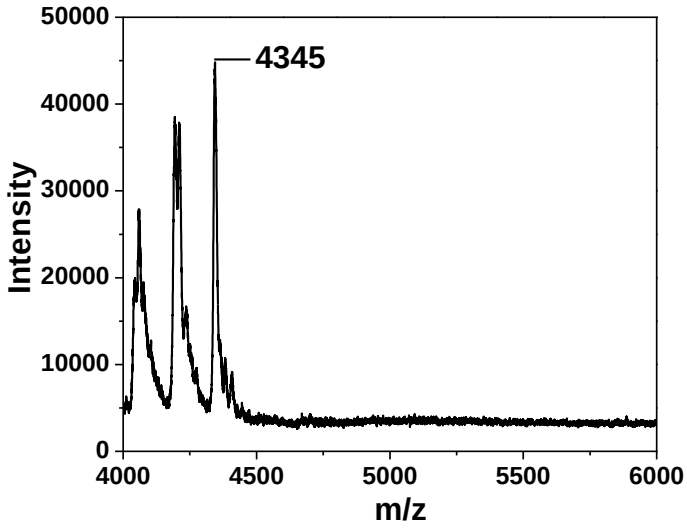

Figure 4.12 MALDI-TOF mass spectrum of T_2 after exposure to 300 µM busulfan.

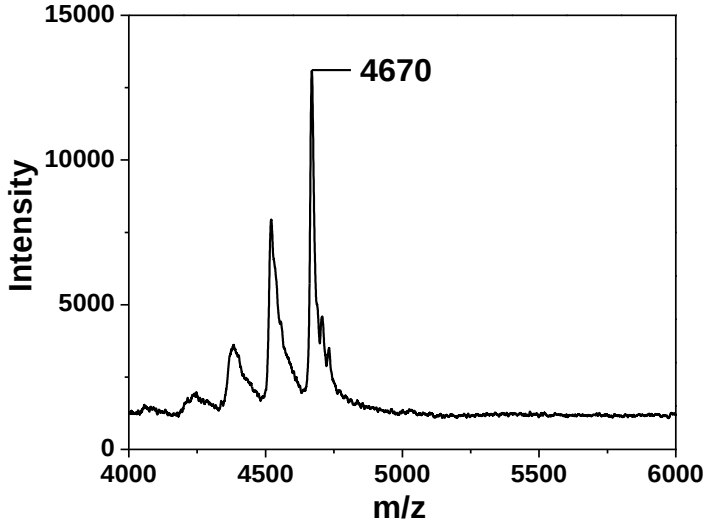

Figure 4.13 MALDI-TOF mass spectrum of control T_3 in the absence of busulfan.

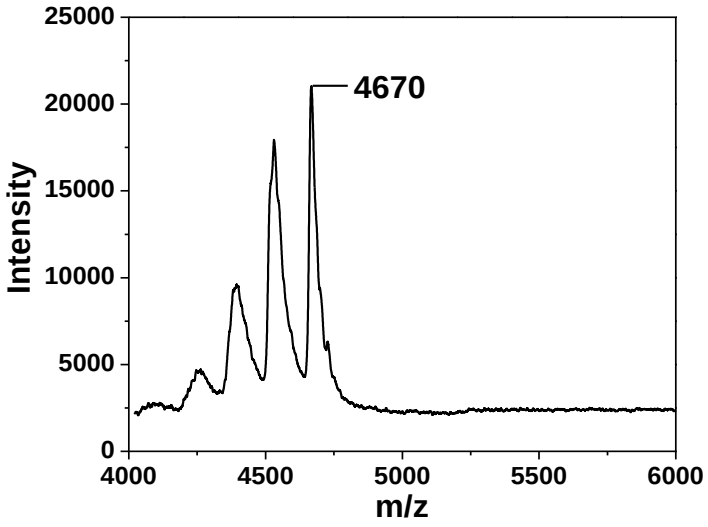

Figure 4.14 MALDI-TOF mass spectrum of T_3 after exposure to 300 µM busulfan.

Figure 4.15 shows the fluorescence intensities in the Cy5 channel of T_1 exposed to different concentrations of busulfan. T_1 has no sites for forming a lesion, so it's hard to judge whether the change in fluorescence is due to damage by busulfan. Also from this figure we can see that there is a significant slide to slide variation because the signals obtained from the control slide are lower than the signals obtained from the other slides treated with different concentrations of busulfan. The same conclusion is derived from Figures 4.16 and 4.17 for T_2 and T_3, respectively. The change in the fluorescence intensities is not due to the effect of busulfan concentration on the lesion sites, because the fluorescence intensities when treating the slides with 300 µM busulfan is higher than the slides treated with 100 µM and 200 µM. So, the change in fluorescence intensities can be due errors from printing ssDNA on the slide surface [31].

Also the slide-to-slide variation makes the comparison more difficult, because the amount of ssDNA printed on the slides is different from spot-to-spot, this is further confirmed in Figures 4.18 - 4.20. These suggested explanations again are supported by the fluorescence FAM signal which is attached to the internal standard.

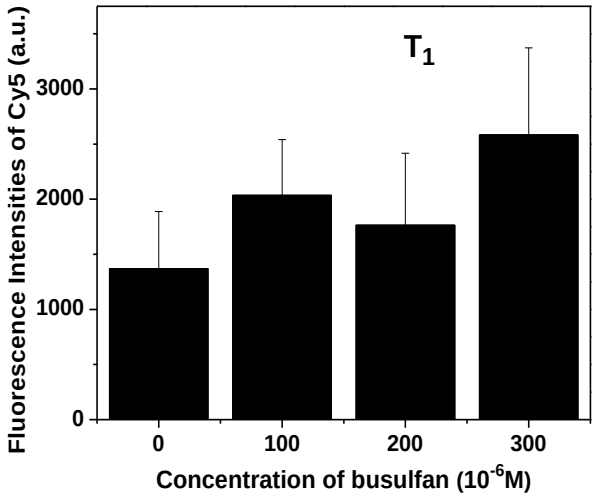

Figure 4.15 Fluorescence intensities of Cy5 channel alone for HP_1 hybridized withT_1 at different concentrations of busulfan.

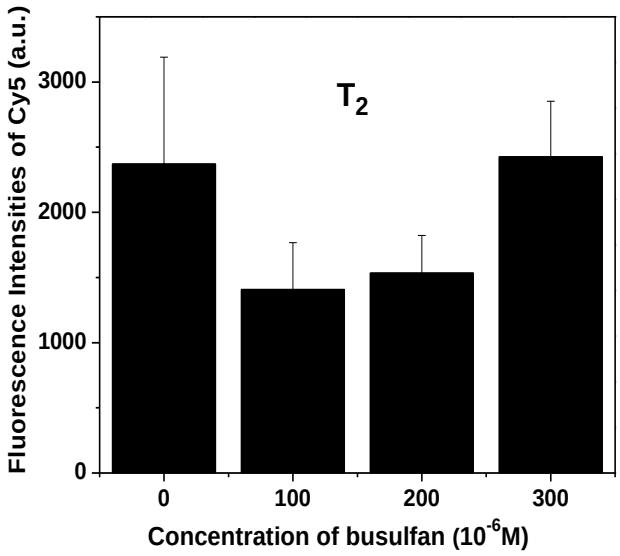

Figure 4.16 Fluorescence intensities of Cy5 channel alone for HP_2 hybridized withT_2 at different concentrations of busulfan.

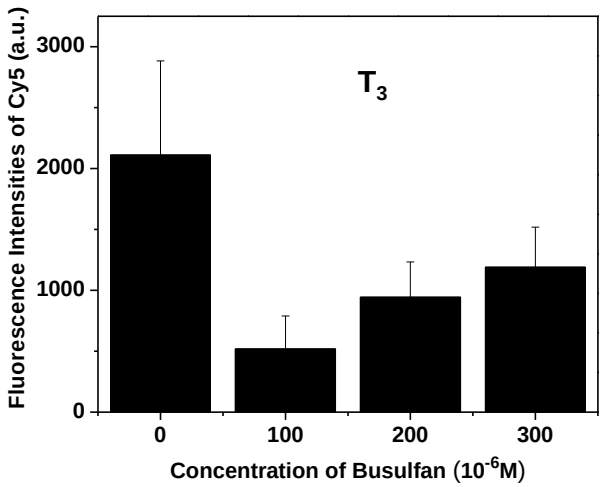

Figure 4.17 Fluorescence intensities of Cy5 channel alone for HP_3 hybridized withT_3 at different concentrations of busulfan.

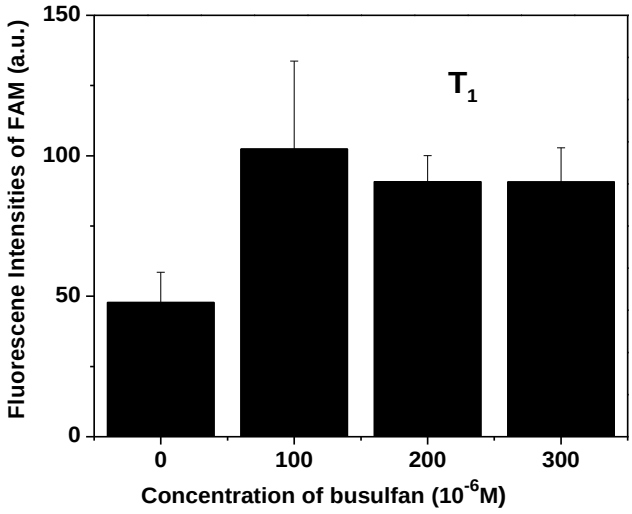

Figure 4.18 Fluorescence intensities in the FAM channel in T_1-subarrays at different concentrations of busulfan.

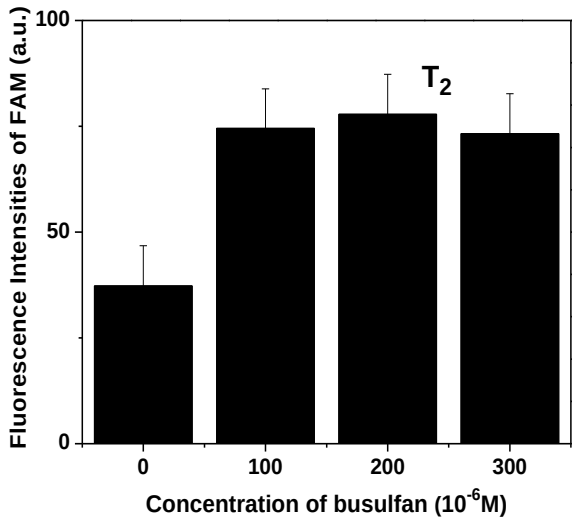

Figure 4.19 Fluorescence intensities in the FAM channel in T_2-subarrays at different concentrations of busulfan.

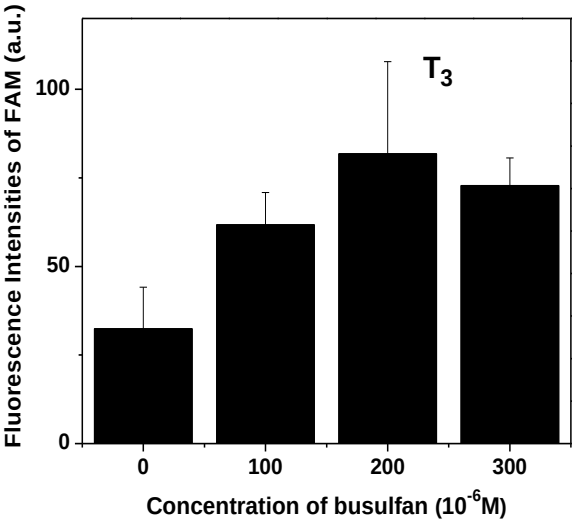

Figure 4.20 Fluorescence intensities in the FAM channel in T_3-subarrays at different concentrations of busulfan.

The first role of the internal standard is as an indicator of the existence of the targets on the slide, and secondly to reduce the error of spot-to-spot printing. In our experiments we are not only exposed to variations of the amount of printed ssDNA from spot-to-spot within one slide, but also to a greater extent from slide-to-slide variation. This is confirmed in Figures 4.18 - 4.20 which show the fluorescence intensities of the FAM channel after treating the slides with BSA and prior to their exposure to busulfan. We can clearly observe that the amount of printed ssDNA is different among the slides, which may make the ratio of I_{Cy5} / I_{FAM} an inappropriate quantity to compare the amount of damaged ssDNA from spot-to-spot let, alone from slide-to-slide.

4.4 CONCLUSIONS

In this Chapter we have demonstrated the use of microarray and fluorescent hairpin probes for the detection of putative chemically-induced DNA damage, specifically from the anticancer drug, busulfan. The data obtained from the microarray analysis showed the ability of surface-attached DNA to study the effect of busulfan on multiple sequences of ssDNA simultaneously. However, the analysis obtained from MALDI-TOF MS suggested that busulfan did not react with the oligonucleotides used in this study because peaks of (target+busulfan) were not observed; therefore the decrease observed in the fluorescence intensities could be due to large errors in the slide-to-slide comparison.

4.5 REFERENCES

1. Díaz, I. P.; Canedo, V. B.; Betanzos, A. A.; Romero, O. F. *Neural Networks*. **2011**, 24, 888-896.

2. Heller, M. J. *Annu. Rev. Biomed. Eng*. **2002**, 4, 129-153.

3. Lander, E. S. *Nat. Genet*. **1999**, 21, 3-4.

4. Wong, L. S.; Khan, F.; Micklefield, J. *Chem. Rev*. **2009**, 109, 4025-4053.

5. Sassolas, A.; Leca-Bouvier, B. D. ; Blum, L. J. *Chem. Rev*. **2008**, 108, 109 -139.

6. Hafemeister, C.; Krause, R.; Schliep, A. *Trans. Comput. Biol. Bioinf*. **2011**, 8, 1642-1651.

7. Fraser, K.; Wong, Z.; Liu, X. *In Microarray Image Analysis. An algorithmic approach*; Blei, D.; Madigan, D.; Melia, M.; Murtagh, F.; Taylor & Francis group: London, 2010; pp 17-51.

8. Young, H. K.; Pollack, J. R. *In Microarray Analysis of the Physical Genome. Methods and protocols*; Pollack, J. R.; Human press: USA, 2009; pp 21-32.

9. Rowe, L. A.; Degtyareva, N.; Doetsch, P. W. *Free Radical Biol. Med*. **2008**, 45, 1167-1177.

10. Britt, A. B. *Plant Physiol*. **1995**, 108, 891-896.

11. Wei, H.; Cal, Q.; Rahn, O. R. *Carcinogenesis*. **1996**, 17, 73-77.

12. Hainaut, P.; Pfeifer, G. P. *Carcinogenesis*. **2001**, 22, 367-374.

13. Steinert, S. A.; Montee, R. S.; Sastre, M. P. *Mar. Environ. Res*. **1998**, 46, 355-358.

14. Buggia, I.; Locatelli, F.; Regazzi, M. B.; Zecca, M. *Ann. Pharmacother*. **1994**, 28, 1055-1062.

15. Probin, V.; Wang, Y.; Zhou, D. *Free Radical Biol. Med.* **2007**, 42, 1858-1865.

16. Iwamoto, T.; Hiraku, Y.; Oikawa, S.; Mizutani, H.; Kojima, M.; Kawanishi, S. *Cancer Sci*. **2004**, 95, 454-458.

17. Bishop, J. B.; Wassom, J. S. *Mutat. Res.* **1986**, 168, 15-45.

18. Morgan, M.; Dodds, A.; Atkinson, K.; Szer, J.; Downs, K.; Biggs, J. *J. Haematol*. **1991**, 77, 529-534.

19. Leadon, S. A.; Hanowalt, P. C. *Mutat. Res.* **1983**, 112, 191-200.

20. Heepchantree, W.; Paratasilpin, T.; Kangwan-pong, D. *J. Toxicol. Environ. Health A*. **2006**, 69, 1071-1082.

21. Karakoula, A.; Evans, M. D.; Podmore, I. D.; Hutchinson, P. E.; Lunec, J.; Cooke, M. S. *J. Immunol. Meth*. **2003**, 277, 27-37.

22. Frelon, S.; Douki, T.; Ravanat, J. L.; Pouget, J. P. ; Tornabene, C.; Cadet, J*. Chem. Res. Toxicol*. **2000**, 13, 1002-1010.

23. Langmaier, J.; Samec, Z.; Samcova, E. *Electroanalysis*. **2003**, 15, 1555-1560.

24. Paleček, E.; Fojta, M.; Tomschick, M.; Wang, J. *Biosens. Bioelectron*. **1998**, 13, 621-628.

25. Kundu, L. M.; Loppnow, G. R. *Photochem. Photobiol.* **2007**, 83, 600-602.

26. Murthy, S. K.; Demetrick, D. J. *Methods Mol. Biol*. **2006**, 319, 237-259.

27. Cahová-Kuchaříková, K.; Fojta, M.; Mozga,T.; Paleček, E. *Anal. Chem*. **2005**, 77, 2920-2927.

28. Broude, N. E. *Encyclopedia of Diagnostic Genomics and Proteomics*. 2005, 846-850.

29. Oladepo, S. A.; Loppnow, G. R. *Photochem. Photobiol*. **2010**, 86, 844-851.

30. Yarasi, S.; McConachie, C.; Loppnow, G. R. *Photochem. Photobiol*. **2005**, 81, 467-473.

31. Vainrub, A.; Pettitt, B. M. *J. Phys. Chem. B.* **2011**, 115, 13300 -13303.

Chapter 5 Conclusions and Future Work

5.1 Molecular beacon probes for the detection of chemically-induced DNA damage.

We have investigated in Chapters 2 and 3 the ability of molecular beacon probes to detect chemically-induced DNA damage via cisplatin and the psoralen derivative HMT, respectively. The results in both cases have shown that the observed decrease in fluorescence signal is due to the mismatch between the targets and the molecular beacon probes. This mismatch is caused by the covalent addition of each agent to the single-stranded DNA. The damage to the ssDNA in both cases is confirmed by MALDI-TOF MS, which shows an increase in mass due to addition of the drug to the ssDNA. Furthermore, the molecular beacon mechanism of action was not disrupted by the presence of excess unreacted drug in solution, which was also confirmed by several control experiments. These results have shown that molecular beacon probes are valid probes for the detection of chemically-induced DNA damage by cisplatin and psoralen.

Early and easy DNA damage detection helps in the fields of drug discovery and cancer treatments as well as prevention. Detection and quantitative measurements of the amount of DNA damaged in cells or tissues due to the exposure of chemical agents help to minimize the cancer risk. MBs are adequate tools to be used in these fields due to their sensitivity and specificity. However, major limitations of these probes are their cost and the sequence specificity requires many probes.

5.2 Detection of chemically-induced DNA damage on a microarray platform.

The use of the microarray tool is beneficial for conducting multiple analyses rapidly and cost-effectively. We have combined this tool with the fluorescent hairpin probe as a sensitive detection method for probing ssDNA exposed to the damaging agent busulfan. The results obtained from scanning the slides exposed to busulfan showed a decrease in the fluorescence signals but the MS measurements of both control and damaged samples were identical, which indicate that there is no addition of busulfan to the ssDNA. So the decrease observed in the fluorescence analysis is not due to damage but due to some other factor, such as errors in printing ssDNA on the slides, which makes the amount in each spot different. Reducing this limitation will be our next step to make DNA microarrays a suitable platform for detecting chemically-induced DNA damage.

DNA microarrays combined with hairpin probes promise a high-throughput method for the analysis of large amount of chemically-induced DNA damage that is fast and cheap. Major limitations of using the microarray platform for the detection of DNA damage is the difficulty in quantifying the amount of damaged DNA attached on the surface, the detection of ssDNA only and its limitation to *in vitro* analysis.

5.3 Future Work

5.3.1 Probing chemically-induced DNA damage for mix-and-read solution-based assays by using molecular beacons.

The next step in using MB probes to detect chemically-induced DNA damage will focus on quantifying the amount of chemical damage in ssDNA. This goal can be approached by investigating a method which can help us to measure the fluorescence signal response as a function of the amount of damaged DNA. From an analytical chemistry aspect, we can obtain the concentration of the damaged ssDNA using MALDI-TOF MS. This choice of a technique is the best for our experiment, because it is a label-free quantitative analysis, doesn't cause damage to our sample and MS is sensitive and can confirm structural identities of the products[1]. The healthy ssDNA samples can be used as a standard for calibration. After measuring the concentrations of the analytes, we can construct a calibration curve that relates the concentrations obtained from the MS measurements to the fluorescence signals of the MBs. UV-absorbance is another alternative, where we can calculate the concentration from the absorbance measurements (and it has been used before in our group for quantitation of UV-induced DNA damage). However, absorbance may suffer from matrix interferences and it's not as sensitive as MS.

Another future goal will be to use molecular beacons for *in vivo* analysis. Since molecular beacons are used to probe single-stranded

DNA, it's challenging to try to use it in the cellular level because DNA naturally exists in the double-strand form. Nevertheless, RNA usually adopts the single-stranded form so it can be probed by MBs inside the cells [2]. RNA has been shown to be damaged by cisplatin [3, 4], which makes it a suitable candidate for future *in vivo* analysis [5]. The cultured cells will be treated with the damaging reagent. Then, the cells are incubated with the modified MBs that facilitate their entry to the cells like a peptide linker attached to the probe[5]. And upon hybridizing with the targets it will generate a signal.

5.3.2 Detection of chemically-induced DNA damage by using microarray as a platform.

In Chapter 4, the use of busulfan as a damaging agent for ssDNA was not a successful choice, because there was no damage detected. For the future, the use of effective damaging agents such as cisplatin and psoralen for DNA in a microarray platform can be tested, because DNA microarrays combined with the specificity of the hairpin probes provide us with a miniaturized, low volume, sensitive, multiplexed and fast tool for detecting chemically-induced DNA damage. This factor may help us to overcome the inhomogeneity of printing ssDNA on the slide [6] by causing an effective damage to the spots exposed to the damaging agent, which makes the decrease in the fluorescence signal due to damage larger than the loss of signal due to errors in printing targets on the slide.

Errors of printing should be minimized by the use of self-quenched probes attached to the slide surface. This method is different than what has been discussed in Chapter 4. The target samples are first exposed to the damaging agent then hybridized with the probes attached to the slide. The probe will still be in the form of a hairpin structure attached to a modified surface like agarose film [7] to provide proper quenching of the fluorophore attached to the probe. By printing the probe on the slide, the errors of detecting damage are minimized because the observed signal will depend on the hybridization of the target and the probe, and the damaging process is done off the slide. Spotted MBs should be distant from each other in order to minimize any internal quenching process possible. The attachment of the probe to the modified slide is done through a linker (poly T or poly A) that is attached to either the fluorophore or the quencher. Also a fluorescent hairpin probe can be attached on a gold surface that quenches the fluorophore [8]. In this experiment, the presence of the target will cause the hairpin to open, giving rise to a fluorescence signal.

Busulfan-induced DNA damaged can be investigated in a solution assay using MB probe. This assay will help us to check whether busulfan can form adducts by monitoring the decrease of the fluorescence intensity of the MB probe.

5.4 REFERENCES

1. Edler, M.; Jakubowski, N; Linscheid, M. *J. Mass Spectrom*. **2006**, 41, 507-516.

2. Bratu, D. P.; Catrina, I. E.; Marras, S. A. *Methods Mol. Biol.* **2011**, 714, 141-157.

3. Jordan, P.; Carmo-Fonseca, M. *Nucleic Acids Res.***1998**, 26, 2831-2836.

4. Rijal, K.; Chow, C. S. *Chem. Commun.* **2009**, 1, 107-109.

5. Nitin, N.; Santangelo, P. J.; Kim, G.; Nie, S.; Bao, G. *Nucleic Acids Res.* **2004**, 32, e58.

6. Vainrub, A.; Pettitt, B. M. *J. Phys. Chem*. *B.* **2011**, 115, 13300-13303.

7. Wang, H.; Li, J.; Liu, H.; Liu, Q.; Mei, Q.; Wang, Y.; Zhu, J.; He, N.; Lu, Z. *Nucleic Acids Res.* **2002**, 30, e61.

8. Cederquist, K. B.; Keating, C. D. *Langmuir*, **2010**, 26, 18273-18280.

Chapter 6 Appendix

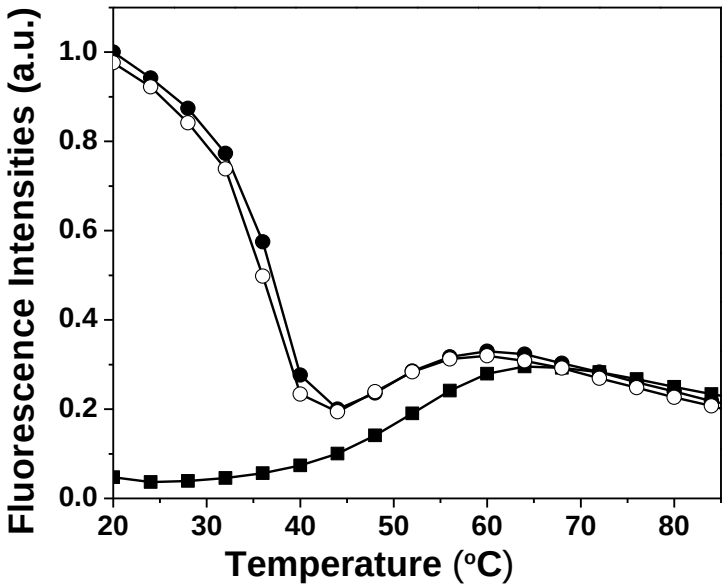

Figure 6.1 Melting curves (heating direction) for 300 nM MB_o : 3 µM undamaged Tgt_o hybrid (filled circles), 300 nM MB_o : 3 µM Tgt_o incubated with cisplatin for 12 hr (open circles), and 300 nM MB_o alone (filled squares). The fluorescence intensities have been scaled to the highest value.

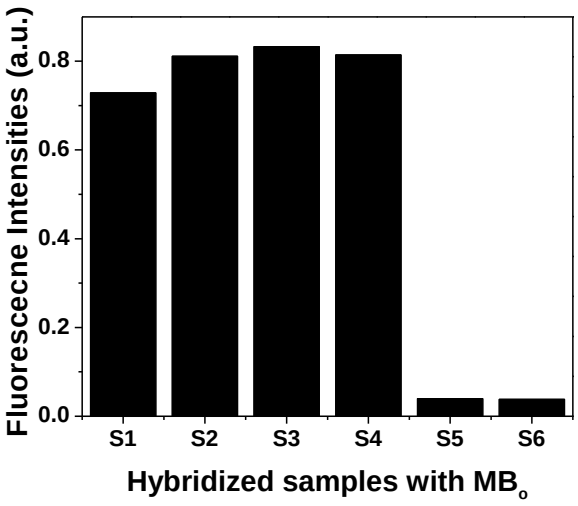

Figure 6.2 Fluorescence intensities of MB_o. Fluorescence intensity of 300 nM MB_o : 3 µM Tgt_o incubated with equimolar of cisplatin for 12 h and then hybridized with MB_o (S_1), fluorescence intensity of 300 nM MB_o : 3 µM Tgt_o (S_2), fluorescence intensity of 300 nM MB_o : 3 µM Tgt_o measured immediately after mixing (S_3), fluorescence intensity of 300 nM MB_o : 3 µM Tgt_o: cisplatin measured immediately after mixing (S_4), fluorescence intensity of 300 nM MB_o alone (S_5), and fluorescence intensity of 300 nM MB_o alone incubated with cisplatin for 12 h (S_6). The fluorescence intensities have been scaled to the highest value.

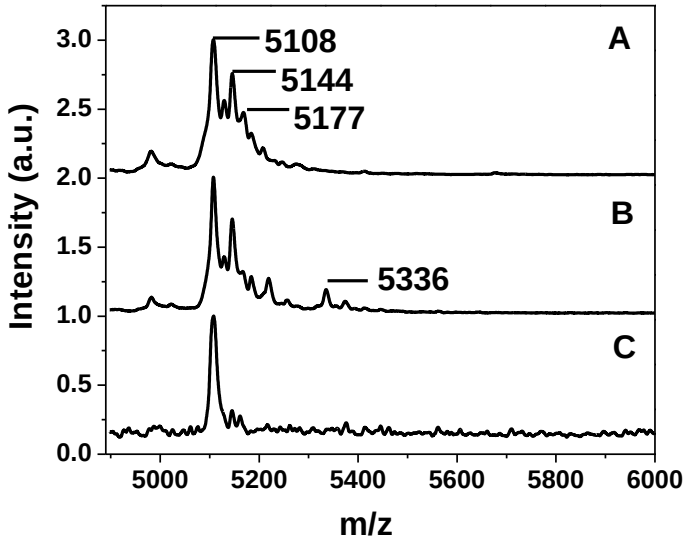

Figure 6.3 MALDI-TOF MS of Tgt_0 oligonucleotide in the absence (A) and presence (B) and (C) of cisplatin. The signals at m/z = 5108 amu indicate the molecular ion of Tgt_0. Spectrum B was taken after the sample mixture of Tgt_0 treated with cisplatin for 12 h and spectrum C was taken immediately after mixing Tgt_0 and cisplatin. The signal in spectrum B at m/z = 5336 amu indicates the addition of one molecule of cisplatin to the target or addition of salts. Smaller peaks in all spectra represent $(Na^+)_n$ or $(K^+)_n$ clusters of the target and adduct(s). The intensities have been scaled to the highest value in each spectrum and offset along the y-axis.

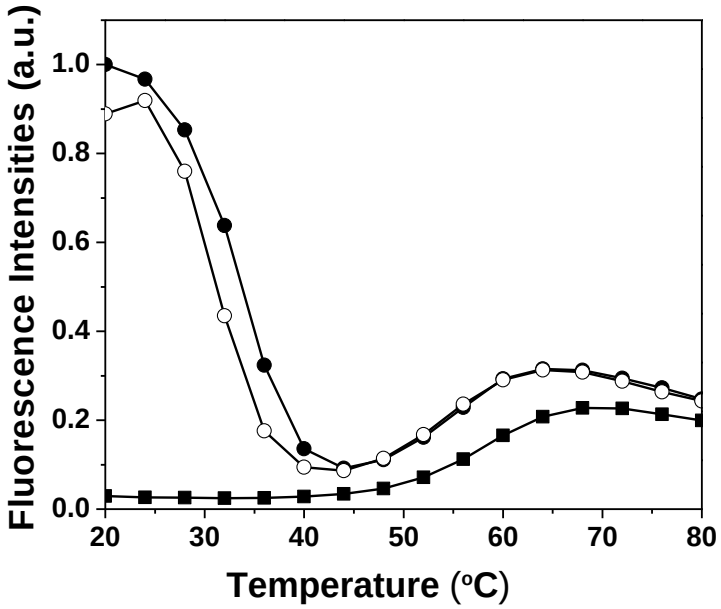

Figure 6.4 Melting curves (heating direction) for 300 nM MB_1 : 3 µM undamaged Tgt_1 hybrid (filled circles), 300 nM MB_1 : 3 µM Tgt_1 incubated with cisplatin (open circles), and 300 nM MB_1 alone (filled squares). The fluorescence intensities have been scaled to the highest value.

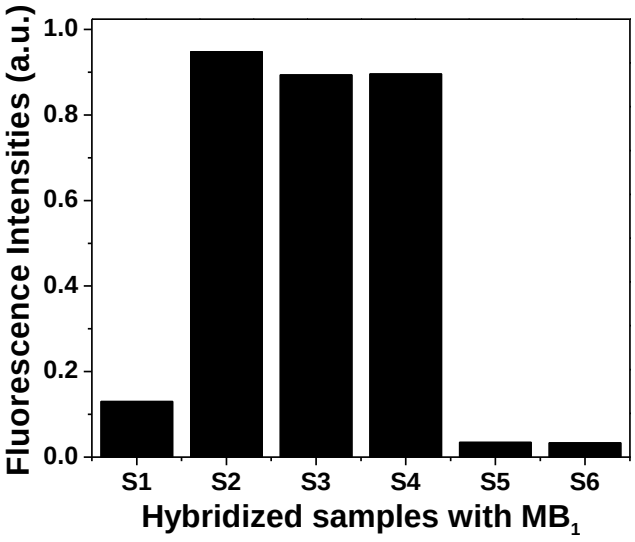

Figure 6.5 Fluorescence intensities of MB_1. Fluorescence intensity of 300 nM MB_1 : 3 µM Tgt_1 incubated with a 2-fold excess of cisplatin for 12 h (S_1), fluorescence intensity of 300 nM MB_1 : 3 µM Tgt_1 incubated for 12 h (S_2), fluorescence intensity of 300 nM MB_1 : 3 µM Tgt_1 measured immediately after mixing (S_3), fluorescence intensity of 300 nM MB_1 : 3 µM Tgt_1: cisplatin measured immediately after mixing (S_4), fluorescence intensity of 300 nM MB_1 alone (S_5) and fluorescence intensity of 300 nM MB_1 alone incubated with cisplatin for 12 h (S_6). The fluorescence intensities have been scaled to the highest value.

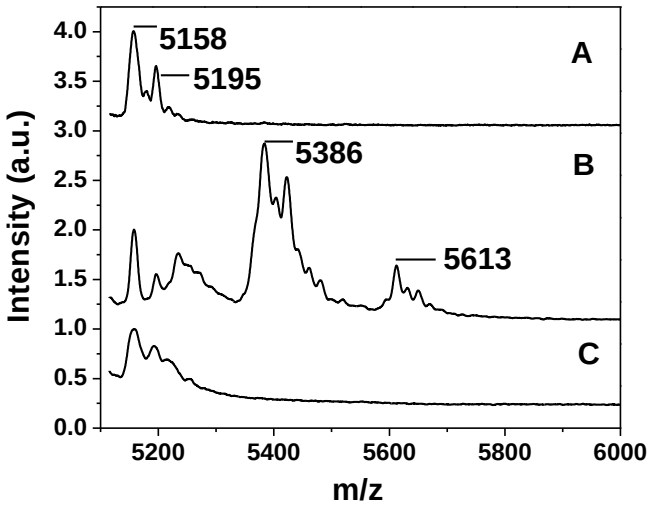

Figure 6.6 MALDI-TOF MS of Tgt_1 oligonucleotides in the absence (A) and presence (B) and (C) of cisplatin. The signals at m/z = 5158 amu in all spectra is the molecular ion of Tgt_1. Spectrum B was taken of Tgt_1 incubated with cisplatin for 12 hr. The signals at m/z = 5386 amu and m/z = 5613 amu indicate the addition of one and two molecules of cisplatin, respectively, to the target. Figure 11C is the spectrum taken immediately after mixing Tgt_1 with cisplatin. Smaller peaks in all spectra represent $(Na^+)_n$ or $(K^+)_n$ clusters of the target and adduct(s). The intensities have been scaled to the highest value in each spectrum and offset along the y-axis.

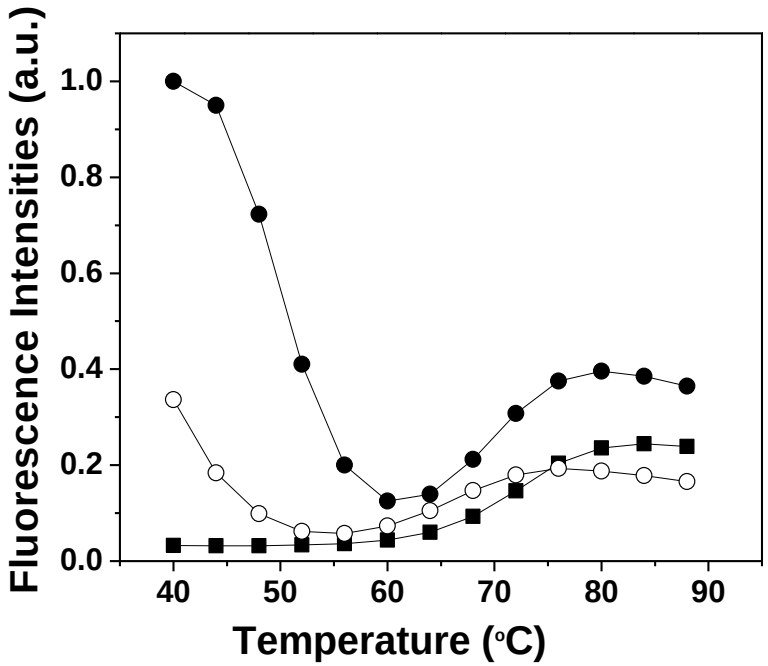

Figure 6.7 Melting curves (heating direction) for the 300 nM MB_{1a} : 3 µM undamaged Tgt_{1a} hybrid (filled circles), for the 300 nM MB_{1a} : 3 µM cisplatin-damaged Tgt_{1a} (open circles), and for the 300 nM MB_{1a} alone (filled squares). The fluorescence intensities have been scaled to the highest value.

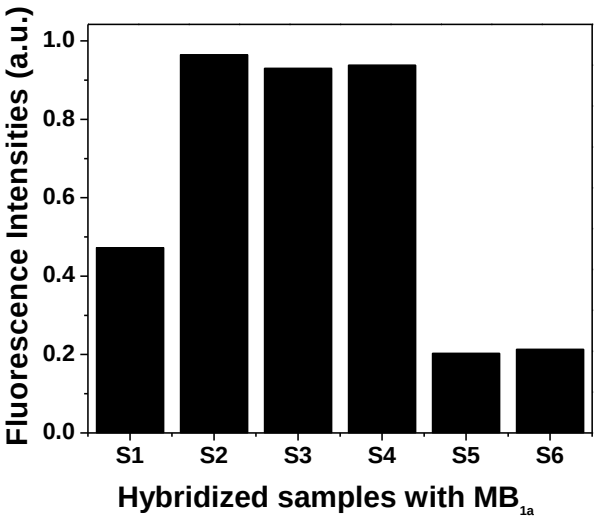

Figure 6.8 Fluorescence intensities of MB_{1a}. Fluorescence intensity of 300 nM MB_{1a} : 3 µM Tgt_{1a} incubated with equimolar cisplatin for 12 h (S_1), fluorescence intensity of 300 nM MB_{1a} : 3 µM Tgt_{1a} incubated for 12 h (S_2), fluorescence intensity of 300 nM MB_{1a} : 3 µM Tgt_{1a} measured immediately after mixing (S_3), fluorescence intensity of 300 nM MB_{1a} : 3 µM Tgt_{1a}: cisplatin measured immediately after mixing (S_4), fluorescence intensity of 300 nM MB_{1a} alone (S_5), and fluorescence intensity of 300 nM MB_{1a} alone incubated with cisplatin (S_6). The fluorescence intensities have been scaled to the highest value.

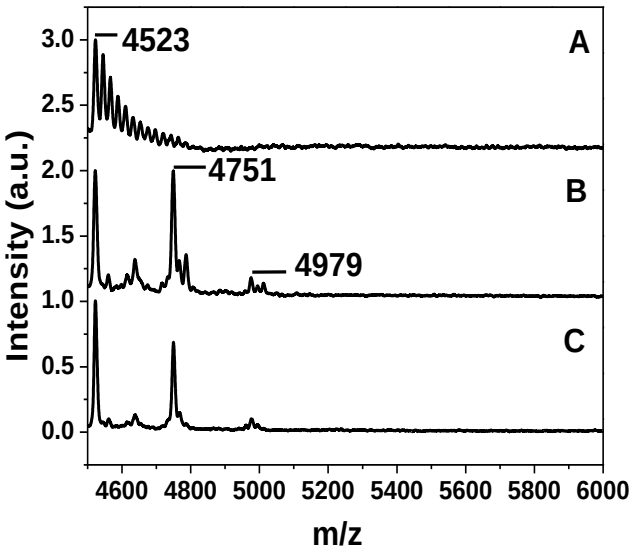

Figure 6.9 MALDI-TOF MS of Tgt_{1a} oligonucleotides in the absence (A) and presence (B) and (C) of cisplatin. The signals at m/z = 4523 amu in all spectra is the molecular ion of Tgt_{1a}. Spectrum B was taken after the sample mixture of Tgt_{1a} was incubated with cisplatin for 12 h. The signals at m/z = 4751 amu and m/z = 4979 amu in spectra B and C indicate the addition of one and two molecules of cisplatin, respectively, to Tgt_{1a}. Smaller peaks in all spectra represent $(Na^+)_n$ or $(K^+)_n$ clusters of the target and adduct(s). The intensities have been scaled to the highest value in each spectrum and offset along the y-axis.

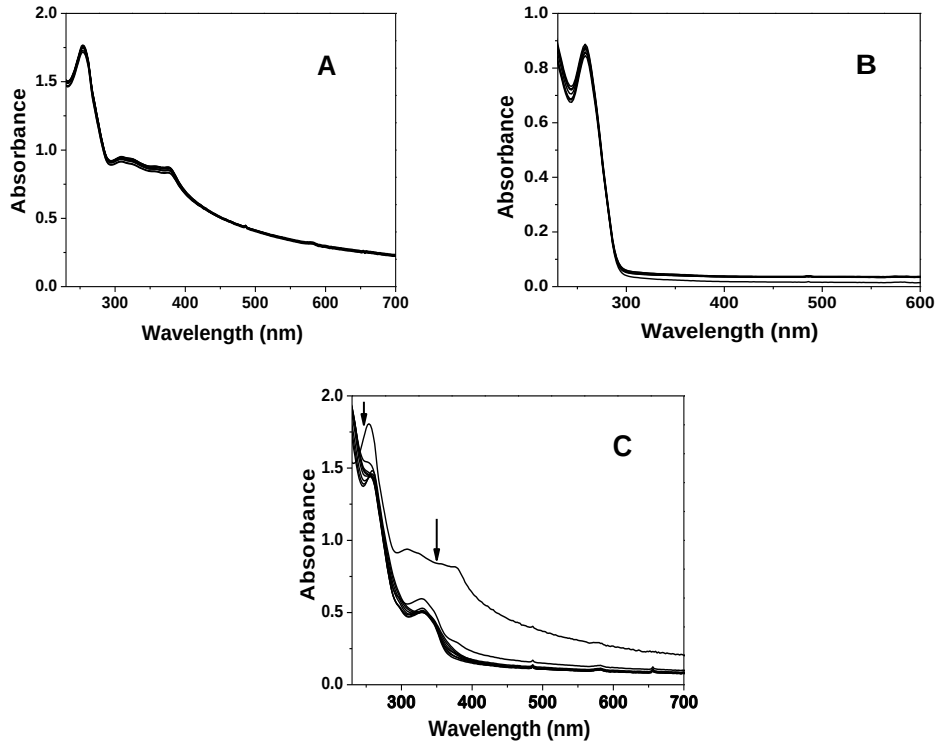

Figure 6.10 UV-Vis absorption spectra of dA_7TTA_8 solutions. (A) is the absorption spectra of a mixture of 3.5 µM dA_7TTA_8 and 100 µM HMT, kept in the dark. (B) is the absorption spectra of solution of 3.5 µM dA_7TTA_8 alone irradiated with UVA light for 0-580 min. (C) is the absorption spectra of a mixture of 3.5 µM dA_7TTA_8 and 100 µM HMT irradiated with UVA light for 0-580 min. In (C), the arrows indicate the direction of absorbance change with increasing irradiation time.

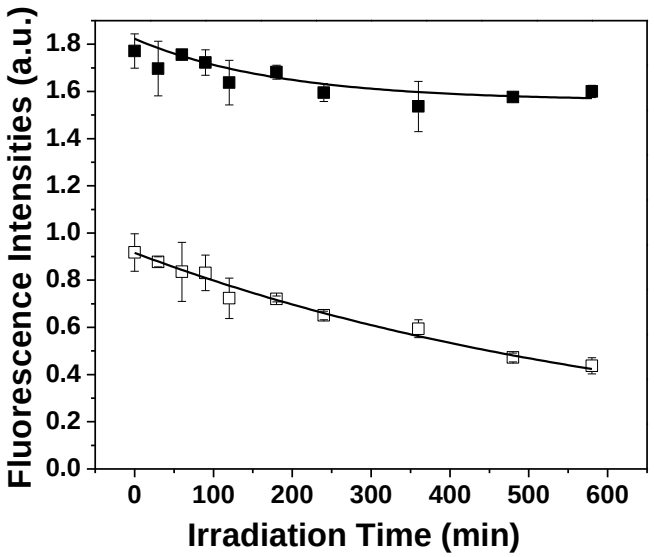

Figure 6.11 Fluorescence intensities of the MB as a function of irradiation time for 100 nM MB incubated with 100 nM dA_7TTA_8 in the presence of HMT irradiated with UVA light. The solid line through the points (filled squares) is an offset, single-exponential $y = yo + Ae^{-x / t1}$ fit. The fluorescence parameters obtained from the fit are $y_o = 50527.3 \pm 1968$, A = 23688 $\pm$ 2046 and $t_1 = 184 \pm 73$ min. The solid line through the points (open squares) is an offset, single-exponential $y = y_o + Ae^{-(x-xo) / t1}$ fit. The fluorescence parameters obtained from the fit are $y_o = 0.059 \pm 0.154$, x_o = 289.2, A = 0.56 and $t_1 = 677.8 \pm 182$ min. Each data point is an average of three replicate measurements and the error bars correspond to the standard deviation of the measurements. The fluorescence intensities have been scaled to the highest value.

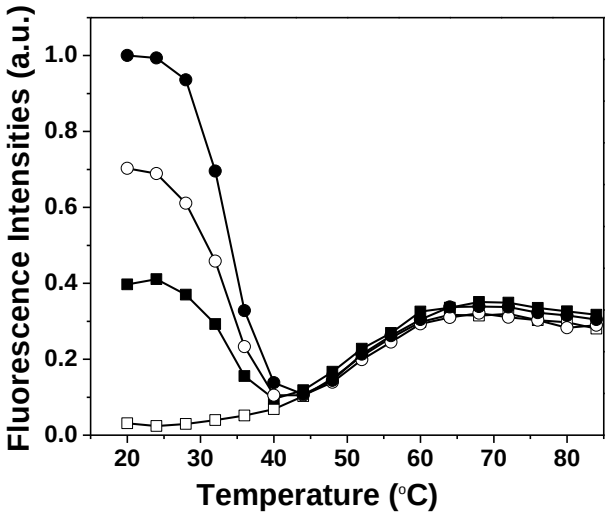

Figure 6.12 Melting curves of 100 nM MB. This figure shows the melting curves of 100 nM MB which was incubated with 100 nM dA_7TTA_8 irradiated for 0 min (filled circles), and similarly for 60 min (open circles), 120 min (filled squares) in the presence of HMT, and 100 nM MB (open squares). The lines are simply guides to the eye. The fluorescence intensities have been scaled to the highest value.

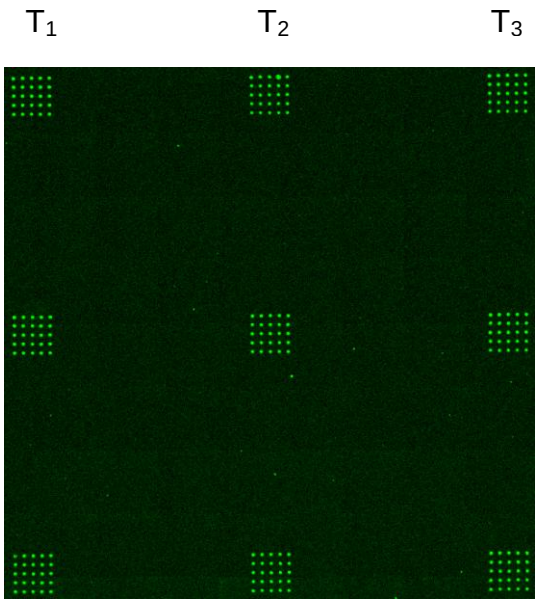

Figure 6.13 Image of the 200 µM busulfan slide after treating the slide with BSA and before treating with busulfan and probe in the FAM channel.

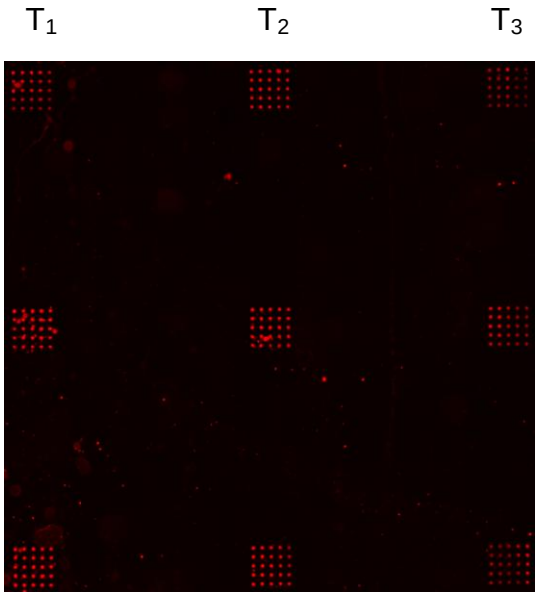

Figure 6.14 Image of the 200 µM busulfan slide treated with busulfan. The image is taken after hybridization with the probe in Cy5 channel.

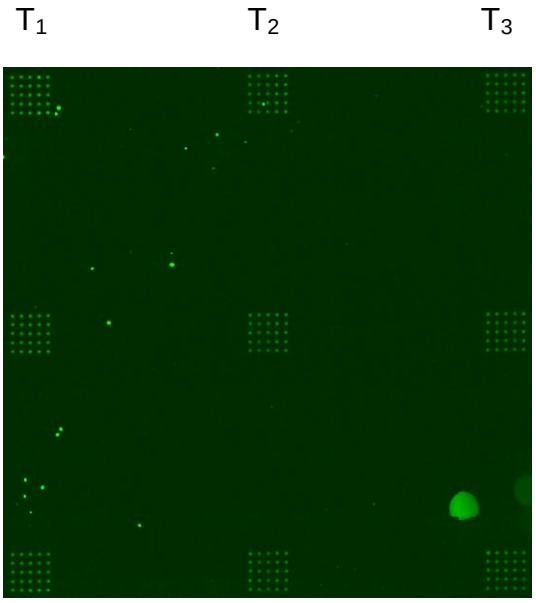

Figure 6.15 Image of the slide treated with 300 µM busulfan. The image is taken after treating the slide with BSA.

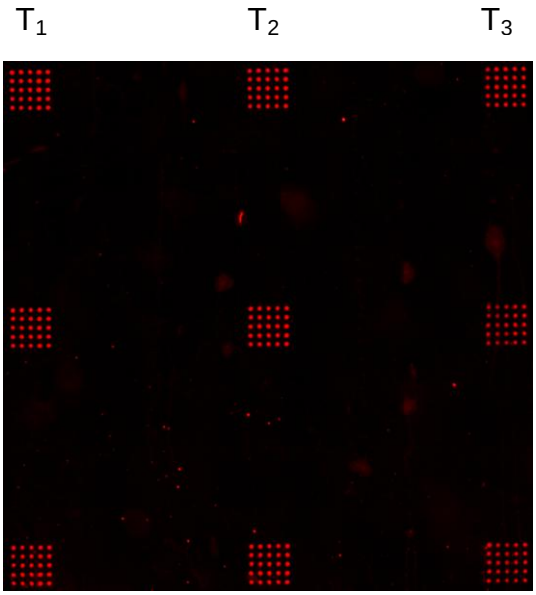

Figure 6.16 Image of the slide treated with 300 µM busulfan. The image is taken after hybridization with the probe.